Heat Shock Factor 1 forms condensates and restructures the yeast genome before activating target genes

Linda S. Rubio, Suman Mohajan, David S. Gross*
Department of Biochemistry and Molecular Biology
Louisiana State University Health Sciences Center
Shreveport, LA 71130

*Corresponding author: david.gross@lsuhs.edu

Keywords: Heat shock response; 3D genome; transcriptional condensates; chromatin; proteotoxicity; ethanol stress; RNA Pol II; *Saccharomyces cerevisiae*

Abstract

In insects and mammals, 3D genome topology has been linked to transcriptional states yet whether this link holds for other eukaryotes is unclear. Using both ligation proximity and fluorescence microscopy assays, we show that in *Saccharomyces cerevisiae*, *Heat Shock Response* (*HSR*) genes dispersed across multiple chromosomes and under the control of Heat Shock Factor (Hsf1) rapidly reposition in cells exposed to acute ethanol stress and engage in concerted, Hsf1-dependent intergenic interactions. Accompanying 3D genome reconfiguration is equally rapid formation of Hsf1-containing condensates. However, in contrast to the transience of Hsf1-driven intergenic interactions that peak within 10-20 min and dissipate within 1 h in the presence of 8.5% (v/v) ethanol, transcriptional condensates are stably maintained for hours. Moreover, under the same conditions, Pol II occupancy of *HSR* genes and RNA expression are detectable only later in the response and peak much later (>1 h). This contrasts with the coordinate response of *HSR* genes to thermal stress (39°C) where Pol II occupancy, transcription, intergenic interactions, and formation of Hsf1 condensates are all rapid yet transient (peak within 2.5-10 min and dissipate within 1 h). Therefore, Hsf1 forms condensates, restructures the genome and transcriptionally activates *HSR* genes in response to both forms of proteotoxic stress but does so with strikingly different kinetics. In cells subjected to ethanol stress, Hsf1 forms condensates and repositions target genes before transcriptionally activating them.

Introduction

Genomes of higher eukaryotes are organized into multiple hierarchical levels. Chromosomes are segregated within individual territories, and within chromosomal territories active and inactive regions are separated into topologically associated domains (TADs) (Wendt & Grosveld, 2014). Within TADs, DNA loops are formed to permit the interaction between enhancers or silencers and the promoters of their target loci. Although this hierarchy suggests a static view of the genome, recent studies have suggested that the genome is quite dynamic, as multiple points of interaction form in response to developmental cues and other stimuli. This dynamic restructuring ranges from the interactions between co-regulated genes (Fanucchi et al., 2013; Papantonis et al., 2012; Park et al., 2014; Schoenfelder et al., 2010), to the convergence of enhancers dispersed across multiple chromosomes into a hub that regulates a single gene (Monahan & Lomvardas, 2015), to the reorganization of the genome that occurs in the zygote (Schulz & Harrison, 2019).

Despite its evolutionary distance, the yeast *Saccharomyces cerevisiae* also possesses an organized genome. Centromeres are located in a cluster at the spindle pole body, while chromosomal arms are extended with telomeres and the nucleolus located at the opposite side of the nucleus (Duan et al., 2010), resulting in a Rabl-like configuration (Taddei & Gasser, 2012). And as in higher eukaryotes, the budding yeast genome is organized into TAD-like structures (Eser et al., 2017) subdivided into smaller loop domains (Hsieh et al., 2015). Also as is the case in mammalian cells, the yeast genome is not static. Genes, including *INO1, GAL1* and *GAL10*, have been observed to reposition from the nuclear interior to the nuclear periphery upon their activation (Brickner et al., 2019; Brickner & Walter, 2004; Cabal et al., 2006; Casolari et al., 2004; Dieppois et al., 2006; Green et al., 2012). In response to methionine starvation, several Met4-regulated genes have been observed to cluster (Du et al., 2017; Lee et al., 2024).

More dramatic still are *Heat Shock Response* (*HSR*) genes under the regulation of Heat Shock Factor 1 (Hsf1). Upon exposure to acute thermal stress (heat shock [HS]), *HSR*

genes dispersed across multiple chromosomes transcriptionally activate and engage in novel *cis*- and *trans*-intergenic interactions between one another – principally although not exclusively involving coding regions – that culminate in their coalescence into intranuclear foci (Chowdhary et al., 2017, 2019). These stress-induced foci, comprised of Hsf1 and components of the transcriptional machinery, form quickly, rearrange rapidly and dissolve suddenly (Chowdhary et al., 2022). As such, Hsf1 clusters exhibit properties of biomolecular condensates, defined as self-organized membrane-free compartments enriched in specific macromolecules that may or may not be phase-separated (Banani et al., 2017). Hsf1 condensate formation elicited by heat shock, like that of *HSR* gene interactions, parallels the kinetics of induction and attenuation of Hsf1-dependent genes (Chowdhary et al., 2017, 2022).

The Hsf1-driven heat shock response is a fundamental, evolutionarily conserved transcriptional program characterized by the gene-specific transcription factor (TF) Hsf1, its DNA recognition element (heat shock element (HSE)) and a core set of target genes encoding molecular chaperones and co-chaperones (reviewed in (Verghese et al., 2012)). In absence of proteotoxic stress, yeast Hsf1 is bound by Hsp70 and its co-chaperone Sis1 in the nucleoplasm (Feder et al., 2021; Krakowiak et al., 2018; Peffer et al., 2019; Zheng et al., 2016). Upon encountering stress, Hsp70 is titrated by unfolded proteins, particularly orphan ribosomal proteins located in the nucleolus and nascent polypeptides in the cytosol (Albert et al., 2019; Ali et al., 2023; Tye et al., 2019; Tye & Churchman, 2021). This results in the release of Hsf1 which then trimerizes and binds to HSEs located upstream of ~50 genes whose transactivation is dependent on this factor (Pincus et al., 2018). Once proteostasis is reestablished, excess Hsp70 binds Hsf1, inactivating it, thereby closing the negative feedback loop that regulates Hsf1 transcriptional activity (Krakowiak et al., 2018; Zheng et al., 2016). Note that in yeast, a fraction of Hsf1 is constitutively trimeric and it is this species that binds high-affinity HSEs even under non-stressful conditions (Giardina & Lis, 1995; Pincus et al., 2018).

In addition to thermal stress, Hsf1 can be activated by chemical stressors such as ethanol. Ethanol is a metabolite of glucose breakdown that budding yeast cells secrete

into their surroundings. Ethanol production helps yeast outcompete other microbes in the environment (Liti, 2015; Piškur et al., 2006; Rozpedowska et al., 2011). Furthermore, once glucose is depleted, ethanol serves as an alternative carbon source (Piškur et al., 2006). Given this strategic use of ethanol, it is of fundamental importance for yeast to have a mechanism in place to respond to the stress that ethanol elicits. Similar to thermal stress, exposure to ethanol causes a large number of cellular perturbations including disruption of the plasma membrane (Piper et al., 1994); disruption of the H^+ ATPase and intracellular acidification (Rosa & Sá-Correia, 1991, 1996; Triandafillou et al., 2020); production of reactive oxygen species (Bandas & Zakharov, 1980; Davidson et al., 1996); depolymerization of the actin cytoskeleton (Homoto & Izawa, 2018; Tan et al., 2017); cell cycle arrest (Johnston & Singer, 1980; Kubota et al., 2004); disruption of mRNP transport to the daughter cell and formation of stress granules (Grouši et al., 2009; Kato et al., 2011); global inhibition of transcription and translation (Bresson et al., 2020; Gasch et al., 2000); and formation of protein aggregates (Piper, 1995; Plesset et al., 1982; Stanley et al., 2010). The cell counteracts many of these perturbations through the enhanced production of molecular chaperones (Altamirano et al., 2024; Verghese et al., 2012).

Here, we investigate activation of the HSR in yeast exposed to 8.5% ethanol (ethanol stress (ES)) and compare it to the response induced by exposure to 39ºC (HS). We find that like HS, exposure to ES induces transcription of Hsf1-regulated *HSR* genes and induces concerted intergenic interactions between them. In contrast to HS, however, Hsf1 condensate formation and *HSR* intergenic interactions cells peak well before transcription. The delay in transcriptional induction may be linked to a widespread increase in nucleosome occupancy that occurs upon exposure of cells to ethanol. At longer times of ethanol exposure, *HSR* gene transcript accumulation continues to increase while *HSR* gene coalescence has already dissipated. Likewise, ES-induced Hsf1 condensates are present for a prolonged period, in contrast to HS-induced condensates that begin to dissipate shortly after they appear. Collectively, our data indicate that different stimuli drive distinct transcription, chromatin, topologic and condensation phenomena, yet all are dependent on Hsf1.

Results

Thermal stress and ethanol stress elicit distinct proteotoxic responses in yeast

Saccharomyces cerevisiae in the wild metabolizes glucose and other sugars into ethanol, which the yeast secretes into the environment to suppress microbial competition. Therefore, it is likely that yeast has evolved mechanisms to contend with ethanol toxicity. Indeed, a common laboratory strain (W303) retains viability when cultivated in the presence of 8.5% ethanol, although its ability to proliferate is diminished (**Figure 1A, B**). As assessed by the presence of Hsp104-containing foci (a measure of protein aggregation (Liu et al., 2010)), the rate of cytosolic protein aggregation is similar in cells exposed to either 8.5% ethanol or 39ºC thermal stress (**Figures 1D and 1E**; see **Figure 1C** for experimental design). However, it is notable that the number and volume of Hsp104 foci, and by extension protein aggregation, is substantially higher in cells subjected to ethanol stress.

We next investigated the subcellular localization of the Hsp70 co-chaperone, Sis1, in cells exposed to ethanol versus thermal stress. Previous work has shown that Sis1 is diffusely localized within the nucleus under control conditions where it promotes binding of Hsp70 to Hsf1, thereby repressing the HSR (Feder et al., 2021). In response to acute HS, Sis1 relocates to nucleolus where it forms a perinucleolar ring, and to the cytoplasm where it forms cytosolic clusters that colocalize with Hsp104 and spatially associate with the endoplasmic reticulum (Feder et al., 2021). Consistent with these previous observations, we observed rapid relocalization of Sis1 in response to a 39ºC HS. It formed a ring-like structure within 2.5 min consistent with a perinuclear location. Such relocalization lasted at least 60 min and spatially separated Sis1 from Hsf1 (**Figures 2A and 2B**). A similar result was obtained when cells were exposed to 42ºC. In response to ES, Sis1 remained largely co-localized with Hsf1 within the nucleoplasm although some enrichment at the nuclear periphery was evident. This was the case whether cells were exposed to 5% or 8.5% ethanol (**Figures 2A and 2B**). In addition, a 60 min exposure to 8.5% ethanol resulted in the formation of prominent cytosolic Sis1 puncta that were less evident in the HS sample (**Figure 2A**). These observations suggest that these two

stressful treatments elicit a qualitatively distinct response. Experiments described below provide further support for this possibility.

Ethanol stress induces transcriptional activation of Hsf1-dependent genes but with delayed kinetics and reduced expression compared to thermal stress

To gain further insight into the mechanism by which *S. cerevisiae* contends with ethanol-induced proteotoxicity, we assessed the kinetics of transcriptional activation of *HSR* genes in cells exposed to ethanol stress. Cells were cultivated to early log phase in rich YPD medium, then ethanol was added to a final concentration of 8.5% and cell aliquots were removed at 0-, 10-, 20- and 60-min. Transcription was terminated through addition of sodium azide (see Materials and Methods). A parallel culture was exposed to an instantaneous 30° to 39°C heat shock and cells were removed at the corresponding time points. Transcription was terminated as above.

While cells exposed to heat shock displayed a rapid and substantial increase in *HSR* mRNA levels (typically >10-fold increase within 10 min of thermal upshift), those exposed to ethanol stress only weakly induced the same cohort of genes (**Figure 3A**). However, while HS induced a transient increase in RNA expression, ES induced a sustained increase that was evident at all Hsf1-dependent genes tested (**Figure 3–figure supplements 1 and 2**). A corresponding immunoblot analysis of two Hsf1 targets, Hsp104 and Btn2, strengthens the notion that HS induces a rapid yet transient response whereas ES induces a delayed, yet far more sustained increase in gene expression (**Figure 3–figure supplement 3**). In the case of *HSP12* and *HSP26*, whose transcription is under the dual regulation of Msn2 and Hsf1, exposure to heat shock resulted in a high level of induction as previously observed (Chowdhary et al., 2019) yet exposure to 8.5% ethanol failed to cause detectable activation during the first 20 min (**Figure 3B; Figure 3–figure supplement 1**). Nonetheless, as described below, both *HSP12* and *HSP26* respond to acute ethanol stress but do so through their inducible and dramatic 3D genomic repositioning.

Pol II recruitment and histone eviction are delayed in ethanol-stressed cells and this correlates with a transient, widespread increase in nucleosome density

The delayed transcriptional response of *HSR* genes in ES- versus HS-treated cells prompted us to investigate occupancy of Hsf1, RNA Pol II and histones at these genes over a time course. A possible explanation for the delay in activation in cells exposed to ethanol stress is less rapid (or reduced) Hsf1 binding to the genes' upstream regulatory regions. To explore this possibility, we exposed cells to either thermal or chemical stress and processed them for chromatin immunoprecipitation (ChIP) analysis. As previously observed (Kim & Gross, 2013; Pincus et al., 2018; Sekinger & Gross, 2001), occupancy of Hsf1 at its target loci increases many-fold following a brief heat shock (**Figure 4B,** left, dark red; see **Figure 4A** for location of primers). Hsf1 occupancy typically declines after 60 min of continuous thermal stress and in the case of *TMA10*, dissociation begins much sooner. In response to ethanol stress, Hsf1 occupancy steadily increased, in most cases reaching maximal levels by 20 min and plateauing thereafter (**Figure 4B,** left, black). These results suggest that ethanol stress induces binding of Hsf1 to its cognate HSEs to a degree similar to heat shock, yet such binding is more gradual. Moreover, given the above, Hsf1's binding to these sites fails to elicit a corresponding transcriptional response.

In light of this disconnect between Hsf1 binding and *HSR* mRNA production, we evaluated abundance of the large subunit of Pol II at representative genes over the same time course. In response to heat shock, Rpb1 is rapidly recruited to the promoters and coding regions of each *HSR* gene, peaking within 2.5 min and then gradually declining over the next ~60 min (**Figure 4B**, middle, red and pink traces). By contrast, its occupancy is noticeably delayed in cells exposed to ethanol stress (blue traces), consistent with reduced transcript levels (**Figure 4–figure supplement 1B**). The increase in *HSR* mRNA in heat-shocked cells parallels, yet consistently lags, the abundance of Pol II within *HSR* gene coding regions (**Figure 4–figure supplement 1A**). This delay in reaching peak accumulation may reflect contributions beyond RNA

synthesis, such as transient enhanced stability of *HSR* transcripts during the acute phase of heat shock.

To obtain further insight into the chromatin landscape present during the two stresses, we assayed histone H3 abundance as a measure of nucleosome density. In response to heat shock, nucleosomes are rapidly displaced over the promoter and coding regions of strongly expressed *HSR* genes (*HSP82, HSP104* and *SSA4);* a similar, albeit less robust, response is observed for *TMA10* and *HSP12*. Following this initial phase (~20 min), nucleosomes reassemble over these genes and in certain cases return to their original density by 60 min (**Figure 4B**, right, red and pink traces). This dramatic and dynamic remodeling has been previously observed (Kremer & Gross, 2009; Zhang et al., 2014; Zhao et al., 2005). In contrast, ethanol stress elicits a transient increase in H3 abundance over all five genes (**Figure 4B**, right, blue traces). This apparent increase in chromatin compaction is not restricted to *HSR* genes; a variety of unrelated loci, including a stress-responsive, Msn2-regulated gene (*PGM2*), two constitutively expressed genes (*TUB1, ACT1*), two genes assembled into *SIR*-dependent heterochromatin (*HMLα1, YFR057w*) and a non-transcribed region (*ARS504*) also exhibit a transient increase in nucleosome density in ethanol-exposed cells (**Figure 4–figure supplement 2A**).

In agreement with this idea, chromatin volume (as assessed by the signal arising from an H2A-mCherry protein fusion) decreases upon exposure of cells to ethanol stress (and much more transiently to heat stress; **Figure 4–figure supplement 2[B, C]**). These data suggest that the increase in nucleosome density antagonizes Pol II recruitment and its subsequent release into the coding regions of *HSR* genes in ES cells. Once Pol II has been stably recruited, elongation and concomitant histone eviction ensues (**Figure 4B**). Altogether, our ChIP data indicate that Hsf1 binds to its target enhancers less readily in ethanol-stressed than in thermally stressed cells. This impediment to Hsf1 occupancy is magnified by a corresponding, and more severe, hindrance to Pol II recruitment resulting in a pronounced delay in *HSR* gene transcription.

Acute ethanol stress induces rapid and profound 3D genomic repositioning of *HSR* loci

An intriguing feature of *HSR* genes is the fact that they coalesce into discrete intranuclear foci in response to heat shock. Such interactions have been documented using both molecular (chromosome conformation capture (3C)) and imaging (fluorescence microscopy) approaches (Chowdhary et al., 2017, 2019, 2022; Rubio & Gross, 2023). Intriguingly, physical interactions specifically involve Hsf1 targets irrespective of their location in the genome. Other loci, including adjacent, transcriptionally active genes, show little or no tendency to interact with Hsf1-dependent genes. Such *cis*- and *trans*-interactions principally involve gene coding regions and are highly dynamic, typically peaking at 2.5 min and dissipating by 30- to 60-min. The kinetics of HS-induced coalescence often, although not always, correlate with kinetics of transcriptional induction; they also parallel the formation of Hsf1 condensates (Chowdhary et al., 2017, 2019, 2022) as discussed further below.

Given these previous observations, we wished to know if ethanol stress induced similar 3D genome restructuring. It seemed unlikely that such topological changes would occur during the initial phase of ES since only weak Pol II occupancy and low *HSR* transcript levels are observed (**Figures 3, 4**). However, as shown in **Figure 5**, exposure to 8.5% ethanol triggered frequent intergenic interactions between Hsf1 targets during the first 10 min as revealed by Taq I-3C, a highly sensitive, quantitative version of 3C (Chowdhary et al., 2020) (see **Figure 5 – figure supplement 1** for location of 3C primers). Both intra- and interchromosomal interactions can be detected. Moreover, the interaction frequencies following this exposure in most cases equaled, and in some instances exceeded, those detected in cells heat-shocked for 2.5 min (**Figures 5A, 5B**), when peak 3C interactions occur in thermally stressed cells (Chowdhary et al., 2017). A detailed kinetic analysis revealed that intergenic interactions elicited by ethanol stress, similar to those induced by thermal stress, are highly dynamic: detectable within 2.5 min, peak shortly thereafter (within 10-20 min) and largely attenuate by 60 min (**Figures 5** and **6A**).

It has been previously suggested that a functional link exists between gene looping and transcriptional activation (Ansari & Hampsey, 2005; O'Sullivan et al., 2004). Indeed, gene loops and other intragenic interactions (Chowdhary et al., 2017) are readily detected within *HSR* genes in cells exposed to ethanol. However, as is the case with intergenic interactions, these topological changes are kinetically uncoupled from both transcription and Pol II occupancy. They are detected quite early (within 2.5 min), peak soon thereafter (at 10 min) and attenuate by 60 min (**Figure 6B** and **Figure 5 – figure supplement 2**). Taken together, our 3C and expression analyses indicate that 3D genomic repositioning and intragenic looping of *HSR* genes precedes the maxima of transcript levels and Pol II occupancy. Moreover, for certain loci (e.g., *HSP12* and *HSP26*), they argue that neither transcription nor Pol II recruitment is required to drive 3D topological changes in these genes. Further evidence in support of this is provided below.

Live cell imaging reveals that *HSR* genes coalesce to a similar degree under ethanol stress and heat stress conditions

To provide an orthogonal line of evidence for *HSR* gene interaction, we employed fluorescence microscopy to image live cells bearing *LacO*-tagged *HSP104* and *TetO*-tagged *TMA10* loci in cells expressing GFP-LacI and TetR-mCherry fusion proteins. Both genes are located on Chromosome XII, on opposite arms, and are physically separated by the nucleolus (100-200 rDNA repeats) that lies between them (Duan et al., 2010) (schematically depicted in **Figure 7- figure supplement 1A**). In the absence of stress, fluorescence signals representing these two genes are typically well-separated (**Figure 7- figure supplement 1B**, 0 min). Upon heat shock, they rapidly converge, usually within 2.5 min. Upon exposure to ethanol, gene convergence is also observed, albeit less rapidly (**Figure 7- figure supplement 1B**; see also below). Despite the slight delay, these results demonstrate that *HSP104* and *TMA10* coalesce in ethanol stressed cells and do so with similar frequency as in thermally stressed cells (**Figure 7- figure supplement 1C**), consistent with the 3C analysis described above.

Having confirmed the physical interaction of Hsf1-dependent genes under ethanol stress, we assessed the transcriptional status of coalesced genes. Our RT-qPCR analysis indicated that the increase in *HSR* mRNA levels in ES-induced cells is delayed compared to those in HS-induced cells (**Figure 3**). To obtain insight into *HSR* gene transcription kinetics in single cells, we integrated a stem loop array (24xMS2) upstream of *HSP104*, allowing production of a chimeric transcript visualized upon binding of the MCP-mCherry fusion protein (Haim et al., 2007). This strain also harbored *LacO*-tagged *HSP104* and *HSP12* genes and expressed GFP-LacI (schematically illustrated in **Figure 7A**). We were unable to detect an MCP-mCherry focus adjacent to *HSP104* under no stress conditions (**Figure 7B;** 0 min), consistent with very low *HSP104* basal transcript levels (**Figure 3A**). Heat shock induced rapid coalescence between *HSP104* and *HSP12*, as well as transcription from *HSP104*. These phenomena were detectable by 2.5 min as a merged signal of the chimeric transcript and the two GFP-labeled genes (**Figure 7B**). This visualization method allowed us to quantify the percentage of the population that is actively engaged in transcription, revealing that during heat shock, transcription and coalescence are positively correlated (**Figure 7[C, F]**). Consistent with this, after *HSP104* transcription declined (10 min HS), so did *HSP104-HSP12* coalescence (**Figure 7 – figure supplement 1D**).

A detailed single cell analysis supports the strong spatiotemporal correlation between *HSR* gene coalescence and transcription in heat-shocked cells (**Figure 7D**). In contrast, under ethanol stress, *HSP104* RNA was not detected until 5-10 min (and in most cases not until 10 min) even though *HSP12* and *HSP104* coalesced as early as 2.5 min (**Figure 7E; Figure 7 – figure supplement 1D**). Indeed, such an analysis suggests temporal uncoupling between *HSR* gene coalescence and *HSR* gene transcription in ethanol stressed cells (**Figure 7F**). Underscoring the disconnect between 3D genome repositioning and transcription is the fact that in ethanol stressed cells, enhanced *HSP12* RNA levels were undetectable until 60 min (**Figure 3B and Figure 3 – figure supplement 1**). Collectively, our RT-qPCR, 3C and imaging data argue that ethanol stress induces striking topological changes in *HSR* genes within the first 10-20 min and

that these are accompanied by a minimal increase in transcript levels. This provides a sharp contrast to heat-shocked cells where there exists a strong temporal correlation between *HSR* gene transcription and *HSR* gene repositioning (**Figure 7F**).

Ethanol stress induces rapid formation of long-lived Hsf1 condensates

Recently, TF condensates have been proposed as a mechanism for transcriptional regulation (Boija et al., 2018; Cho et al., 2018; Hnisz et al., 2017; Nair et al., 2019; Sabari et al., 2018). Heat shock-activated Hsf1 forms small nuclear condensates (diameter of ≤300 nm) that localize at *HSR* gene loci in both human (Zhang et al., 2022) and budding yeast cells (Chowdhary et al., 2022), and their presence positively correlates with *HSR* gene transcriptional activity. The tendency of Hsf1 to form condensates may be linked to its extensive intrinsically disordered structure (**Figure 8A**), a feature proposed to be critical for the biomolecular condensation of proteins (reviewed in (Alberti et al., 2019; Banani et al., 2017)). Additionally, nuclear stress bodies comprised of HSF1 bound to satellite III DNA repeats in human cells have been described (Jolly et al., 1997, 2002), although formation of these large foci (diameter of several μm) is independent of the sites of active *Heat Shock Protein* genes and their presence may repress *HSR* gene activation (Gaglia et al., 2020).

Given the temporal link between Hsf1 condensation and transcription established in heat-shocked yeast cells, we anticipated that the appearance of Hsf1 condensates in ethanol-stressed cells would be delayed relative to what is seen in heat-shocked cells. However, we found that ethanol stress induced formation of Hsf1-GFP condensates as rapidly as did heat shock. These were visible in virtually all ES cells as early as 2.5 min, paralleling their rapid appearance in HS cells (**Figure 8 B-D**). However, in contrast to the rapid dissolution of condensates in HS cells, those formed in cells exposed to 8.5% ethanol showed no evidence of dissipating even after 60 min of continuous exposure (**Figure 8B, D**). An independent analysis of Hsf1 tagged with a monomeric GFP, mNeonGreen, gave virtually identical results: >90% of cells exhibited Hsf1 puncta as early as 2.5 min and such puncta were stably maintained for 150 min (**Figure 8 – figure**

supplement 1). Moreover, in a further analysis they were still visible at 5.5 h (data not shown). Therefore, in 8.5% ethanol-stressed cells, formation of Hsf1 condensates is uncoupled from *HSR* gene transcription and their maintenance is uncoupled from *HSR* gene repositioning. An important implication is that although condensates may initiate or promote *HSR* gene repositioning, they cannot maintain the 3D restructured state of the genome.

Does the enhanced stability of ES-induced puncta arise from the nature of the stress or its intensity? To test this, we examined the behavior of yeast cells exposed to a lower concentration of ethanol. As shown in **Figure 8 – figure supplement 1**, Hsf1 puncta formed in >95% of 5% ethanol-treated cells within 2.5 min, resembling what was seen in cells exposed to either 8.5% ethanol or 39°C HS. Yet such puncta dissipated in a majority of 5% ES cells within 30 min, resembling the case with HS but strongly contrasting to what was seen with 8.5% ethanol. Therefore, although 5% and 8.5% ES elicit a similar pattern of Sis1 subcellular relocalization, one that is distinct from that caused by either a 39° or 42°C HS (Figure 2), it is the greater intensity of 8.5% ethanol stress, not its intrinsic nature, that most closely correlates with the stability of Hsf1 condensates.

Hsf1 and Pol II are required for *HSR* gene interactions in response to both heat shock and ethanol stress

The above analyses reveal several unexpected differences in the way yeast responds to ethanol stress versus heat stress. Given these differences, we asked whether either Hsf1 or RNA Pol II are required for the repositioning of *HSR* genes in response to ethanol stress; both have been shown to be necessary for 3D genome restructuring in response to heat shock (Chowdhary et al., 2019, 2022). To do so, we used the auxin-induced degradation system to conditionally degrade Hsf1 and the Rpb1 subunit of RNA Pol II in appropriately engineered strains. As schematically summarized in **Figure 9A**, cells expressing degron-tagged Hsf1 or Rpb1 were pre-treated with 1 mM indoleacetic acid (IAA) for 30-40 min, at which time each protein was >90% degraded (**Figure 9 –**

figure supplement 1A). Although minimal short-term growth defects were detectable, loss of Rpb1 and Hsf1 resulted in loss of cell viability at all temperatures (**Figure 9 – figure supplement 1 [B, C]**).

Consistent with previous observations (Chowdhary et al., 2019), intergenic interactions between *HSR* genes, located on the same or different chromosomes, were nearly obviated in cells conditionally depleted of either Hsf1 or Rpb1 and then heat shocked (**Figure 9B** and data not shown). While a similar strong dependence on Hsf1 is observed in 8.5% ethanol-treated cells, close inspection of the data suggests that residual *HSR-HSR* gene interactions are retained in Rpb1-depleted cells for certain loci. Particularly noteworthy is the inducible interaction between *HSP12* and *HSP26*, genes co-regulated by Msn2 and Hsf1. Neither is detectably activated following a 10-min exposure to ethanol (**Figure 3B**), yet the genes engage in an intergenic interaction that is unaffected by prior degradation of Rpb1 (**Figure 9B**). Together with the kinetic uncoupling of *HSR* gene repositioning with Pol II recruitment/transcription and the relative permanence of Hsf1 condensates described above, these observations raise the possibility that 8.5% (v/v) ethanol-induced Hsf1 condensates are compositionally different from those formed in response to heat shock and drive *HSR* gene repositioning and transcription in a mechanistically distinct way (see **Figure 10** for model).

Discussion

Ethanol stress induces *HSR* gene transcription, *HSR* gene coalescence and formation of Hsf1 condensates

Here we have shown that exposure of budding yeast to a high, but sub-lethal, concentration of ethanol strongly stimulates the binding of Hsf1 to the upstream regulatory regions of *HSR* genes. Unexpectedly, such binding – which is evident as early as 2.5 min – does not lead to concurrent recruitment of Pol II and transcription of *HSR* genes. Instead, Pol II recruitment and transcription are delayed, typically for 10 min or longer. As exposure to 8.5% ethanol causes a global yet transient increase in H3

occupancy – which we interpret as an increase in the compaction of chromatin (see below) – the increase in nucleosome density may present a barrier to both Pol II recruitment and elongation. In addition, another feature of heat shocked-induced Hsf1 activation, repositioning of *HSR* genes within the 3D genome, is observed in cells exposed to ethanol. However, unlike transcription, this phenomenon occurs rapidly and is transient, resembling what is observed in heat shocked cells. The lack of temporal linkage between *HSR* gene transcription and *HSR* intergenic interactions is consistent with the idea that *HSR* gene coalescence and transcription are distinct phenomena and that Hsf1 can instigate long-range changes in 3D genome structure independently of inducing transcription. Thus, Hsf1 represents an example of a gene-specific TF that has functions independent of regulating transcription (discussed further below).

It has recently been demonstrated that in response to heat shock, inducible transcriptional condensates drive 3D genome reorganization in budding yeast. This conclusion arose from several features, including the tight temporal linkage between Hsf1 condensation and *HSR* intergenic interactions and the similar sensitivity of these two phenomena to the aliphatic alcohol, 1,6-hexanediol (Chowdhary et al., 2022). Similar to previous observations of heat-shocked cells (and confirmed here), we have found that in cells exposed to 8.5% ethanol, Hsf1 forms discrete puncta within 2.5 min. However, Hsf1-containing condensates formed in response to 8.5% ES are stable – persisting for hours – while such assemblies dissipate within 30 min in cells exposed to HS. In addition, while Hsf1 condensates formed as rapidly in cells exposed to 5% versus 8.5% ethanol, those formed in the presence of 5% ethanol proved to be transient, resembling their counterparts in HS cells. Relevant to this observation is the finding that Hsf1 activation in yeast exposed to 5% ethanol is dependent on the misfolding of nascent proteins, while in cells exposed to 8% ethanol, Hsf1 activation is dependent on the misfolding of both nascent and mature proteins (Tye & Churchman, 2021). Therefore, the persistence of Hsf1 condensates in 8.5% ethanol may derive from widespread unfolded mature proteins that are more difficult to refold than short nascent polypeptides attached to ribosomes.

Additional features might account for the way in which these two proteotoxic stresses elicit the HSR in budding yeast. For example, while ethanol denatures proteins similar to thermal stress (Furutani & Izawa, 2022; Kato et al., 2011), it impacts the cell at other levels. Actively growing yeast preferentially consume sugars and even in the presence of oxygen can produce ethanol (Dashko et al., 2014). This change in carbon source, termed the diauxic shift, is marked by a reduction in growth rate due to the less efficient generation of energy as well as accumulation of waste products and depletion of nutrients (Herman, 2002). Consistent with activation of the HSR, this physiological adjustment is accompanied by increased chaperone synthesis (Piper, 1995; Piper et al., 1994) as well as an increase in the activity of alcohol metabolism-related enzymes. Such an adaptation likely takes time. In contrast to the gradual increase in ethanol that occurs under natural conditions, here we have imposed an instantaneous ethanol shock. The addition of ethanol elicits a heat shock transcriptional response and synthesis of chaperones. The cell growth arrest seen here (**Figure 1A**) may arise as part of the adaptive program deployed upon encountering ethanol stress, such as a transition into quiescence. However, we fail to see activation of Msn2 targets, a signature of quiescence (Breeden & Tsukiyama, 2022), early in the exposure to ES at a time when Hsf1 itself is activated (**Figure 3B**). While other possibilities exist, our results suggest that the activation of programs involved in proteome protection are likely the first line of defense against sudden ethanol stress. Salient differences by which yeast cells respond to heat versus ethanol stress are summarized in **Table 1**; a model summarizing the Hsf1 response under both HS and ES conditions is provided in **Figure 10**.

Exposure to ethanol transiently induces the global compaction of chromatin

An important observation is that exposure of cells to 8.5% ethanol leads to a widespread increase in H3 ChIP signal that we interpret as increased compaction of chromatin. Although this effect is temporary, both euchromatic and heterochromatic regions are impacted, and this is consistent with measurements of total chromatin volume that reveal a decrease lasting nearly 60 min. A similar outcome was recently

reported for both yeast and mammalian cells exposed to aliphatic di-alcohols (Itoh et al., 2021; Meduri et al., 2022). It is probable that the effect of ethanol exposure is nearly instantaneous since, as discussed above, ethanol is known to denature proteins (Kato et al., 2019), likely by dehydration (disruption of biomolecules' hydration shell). While such denaturation may contribute to chromatin compaction, the effect is reversible, possibly due to refolding / renaturation mediated by Hsp70 and other molecular chaperones whose intracellular concentration increases during ethanol exposure. As mentioned above, this temporary increased density of chromatin could suppress Pol II recruitment and subsequent elongation. Also not ruled out is a direct effect of 8.5% ethanol on one or more components of the Pol II machinery. Possible advantages of chromatin compaction could be to downregulate global transcription, as well as to limit chromatin damage by reactive oxygen species or other potentially damaging molecules present in the cell during ethanol stress (Bradley et al., 2021; Costa et al., 1997; Davidson et al., 1996; Davidson & Schiestl, 2001; Shen et al., 2020; Voordeckers et al., 2020).

A novel function for a TF that is uncoupled from regulating the transcription of its target gene

A key finding is that in response to ethanol stress, *HSR* genes reposition and Hsf1 condensates form well before transcription of Hsf1-dependent genes peaks, and in certain cases, is even detected. This suggests that Hsf1 has a function distinct from transactivating its target genes: it drives *HSR* gene repositioning that culminates in their physical coalescence. Likewise, deletion of the N-terminal IDR (NTA, amino acids 1-140; see **Figure 8A**) was observed to have little effect on *HSR* gene transcription during an acute heat shock yet formation of Hsf1 condensates and intergenic 3C interactions were suppressed (Chowdhary et al., 2022). Furthermore, as discussed above, recruitment of Hsf1 to its target HSEs is delayed in response to ES versus HS. Nevertheless, formation of Hsf1 condensates occurs with similar kinetics under both conditions, well prior to the peak of Hsf1 DNA binding in ES cells. This suggests the possibility that two types of Hsf1 clusters exist: one that is DNA-bound and the other

that hovers over the *HSR* genes. It is possible that this cloud-forming Hsf1 cluster aids in target searching, by analogy with Gal4 that can also form clusters without binding DNA (Meeussen et al., 2023).

Conclusion

While Hsf1 is known to induce interactions between transcriptionally active *HSR* genes in response to heat shock, here we have demonstrated a similar role for this transcription factor in response to ethanol stress. Despite minimal *HSR* gene transcription during the initial 10 min exposure to ethanol, *HSR* genes engage in robust physical interactions, rivaling those seen for 2.5 min HS. This interaction correlates with an increase in definition of Hsf1 condensates yet is not accompanied by concurrent recruitment of Pol II to promoters, perhaps due to the compaction of chromatin in ethanol-stressed cells. Hsf1 therefore forms condensates and drives 3D repositioning of its target genes without appreciably activating these genes. Furthermore, Hsf1 does this through formation of condensates that may be materially different than those that form in response to HS. Our results also argue that formation of TF clusters, while sufficient for TF DNA binding and 3D genome restructuring, are not sufficient to drive transcription. Additional factors and/or activities – such as the opening of chromatin – are necessary. Further research into the biophysical properties, molecular regulation, and functional consequences of HSF1 condensates will deepen our understanding of how cells respond to both thermal and chemical stress and maintain cellular homeostasis.

Materials and Methods

Yeast Strain Construction

The *HSF1-mNeonGreen* (*HSF1-mNG*) diploid strain LRY033 expressing a yeast-optimized version of mNeonGreen, derived from *Branchiostoma lanceolatum* (Shaner et al., 2013), and co-expressing Sis1-mKate and Hsp104-BFP (Blue Fluorescent Protein; mTagBFP2) was created as follows. First, DPY1561 (Feder et al., 2021) was crossed to

W303-1B to create strain LRY031. This diploid was sporulated and a strain homozygous for *HSF1* and retention of one allele each of *SIS-mKate* and *HSP104-mTagBFP2* was obtained after back crossing. The resultant diploid was named LRY032. LRY032 was transformed with a PCR amplicon containing 50 bp of homology sequences flanking the stop codon, targeting the mNG tag to *HSF1* at its C-terminus flanked by the *HIS3* selectable marker. The plasmid template for this amplification was pFA6a-link-ymNeonGreen-SpHis5 (Botman et al., 2019). LRY033 is heterozygous for *HSF1-mNG, SIS1-mKate* and *HSP104-mTagBFP2.*

Other strains were created as follows. LRY037 was constructed using the *HSF1*-targeted *mNeonGreen* amplicon to transform strain W303-1B. LRY040 was constructed by transforming LRY037 with an amplicon containing *RPB3-mCherry::hphMX6*, obtained using genomic DNA from strain SCY004 (Chowdhary et al., 2022) as template. LRY100 and LRY102 were constructed using LRY016 (Rubio & Gross, 2023) as recipient of the mini-degron tag amplified from pHyg-AID*-9myc (Morawska & Ulrich, 2013), targeted to the C-terminus of *HSF1* and *RPB1*, respectively.

A complete list of strains as well as plasmids and primers used in strain construction are listed in **Supplemental File 1 – Tables 1, 2, 3**.

Yeast Culture and Treatment Conditions

Cells were grown at 30°C in YPDA (1% w/v yeast extract, 2% w/v peptone, 2% w/v dextrose and 20 mg/L adenine) to mid-log density (OD_{600}= 0.6 – 0.8). For ethanol stress, the cell culture was mixed with an equal volume of YPDA containing 17% v/v ethanol (yielding a final concentration of 8.5%) and incubated at 25°C for different lengths of time as indicated in the figures. For heat shock, the mid-log culture was mixed with an equal volume of 55°C YPDA medium to achieve an instantaneous temperature upshift to 39°C, and the culture was maintained at 39°C for the indicated times. The no stress samples were diluted with an equivalent volume of YPDA and maintained at 25°C. Samples were kept at their respective temperatures using a water bath with constant shaking.

Cell Viability and Growth Assays

Cell Viability Assay

Cells were grown at 30°C in YPDA to OD_{600}=0.6 and then diluted to OD_{600}=0.4 using an equivalent volume of medium as described above for ethanol stress, heat shock or the no stress control (YPDA at 25°C). Cells were kept under these conditions for 3 h; during this time aliquots were taken at different timepoints and diluted 1:26,000 for plating onto YPDA. Plates were incubated at 30°C for 3 days then scanned. Colonies were quantified using ImageJ/Fiji (v. 1.53t) (Schindelin et al., 2012) - "Analyze Particles" option. The number of colony-forming units (CFUs) obtained in stress samples were normalized to the no stress samples and expressed as a percentage of the number of CFUs obtained in the no stress sample.

Growth Assay

Cells were grown in liquid culture and subjected to the same treatments as described above. OD_{600} readings of each sample were taken at intervals over 3 h (see Figure 1). The average OD_{600} from two samples was plotted versus time.

Spot Dilution

Spot dilution was conducted as described previously (Rubio & Gross, 2023).

Auxin Induced Degradation

Cells expressing the F-box protein osTIR1 in combination with a degron-tagged protein were grown in YPDA medium to mid-log phase and indole-3-acetic acid (IAA) was then added to a final concentration of 1 mM IAA stocks [10 mg/mL (57 mM)] were prepared fresh in 95% ethanol and filter-sterilized before use. For immunoblot analysis, cells were treated for varying times up to 1 h prior to metabolic arrest using 20 mM sodium azide, followed by cell harvesting. 0 min control samples were treated with vehicle alone (1.7% v/v ethanol). For growth curve analysis, samples were kept at 30°C with constant shaking and aliquots were removed at various timepoints to monitor OD_{600}. For 3C analysis, cells were similarly grown in YPDA to OD_{600}=0.6, then treated with 1 mM IAA for either 30 min (LRY016 and LRY100) or 40 min (LRY102) prior to cell cross-linking and subsequent cell harvesting.

Reverse Transcription-qPCR (RT-qPCR)

RT-qPCR was conducted as previously described using 25 mL cell culture aliquots (Rubio & Gross, 2023). Transcription was terminated via addition of sodium azide to a final concentration of 20 mM (Lee & Garrard, 1991). PCR primers used are listed in **Supplemental File 1 – Table 4**.

Immunoblot Analysis

Immunoblotting was performed as previously reported using 20 mL cell culture aliquots (Rubio & Gross, 2023).

Chromatin Immunoprecipitation

Chromatin immunoprecipitation was performed as previously described (Chowdhary et al., 2019) with modifications. Briefly, cells from a 50 mL mid-log culture were exposed to 8.5% v/v ethanol and fixed using 3.01% formaldehyde (HCHO), resulting in a net concentration of 1%. Glycine was then added to 0.363 M glycine to quench excess formaldehyde. We note that HCHO is consumed in a reaction with ethanol. Since 8.5% ethanol equals 1.46 M, acetal formation at 1:2 stoichiometry consumes 0.730 M (2.01%) of HCHO, leaving an effective concentration of 0.363 M (1%). The reaction resulting in formation of an acetal is illustrated in **Figure 11**.

For heat shock, cells from a 50 mL mid-log culture were fixed with 1% (0.363 M) formaldehyde following 39°C upshift for the times indicated (**Figure 4; Figure 4 – figure supplements 1 and 2**). Glycine was then added at a final concentration of 0.363 M to quench unreacted formaldehyde. Chromatin lysates, prepared as previously described (Chowdhary et al., 2019), were incubated using 20% of the lysate with one of the following antibodies: 1.5 µL of anti-Hsf1 (Erkine et al., 1996), 1.5 µL anti-Rpb1 antiserum (Zhao et al., 2005), or 1 µL of H3 antibody (Abcam, ab1791). Incubation of lysate with antibody was done for 16 h at 4°C. Chromatin fragments bound to antibody were captured on Protein A-Sepharose beads (GE Healthcare) for 16 h at 4°C. Wash, elution, and DNA purification were conducted as described (Chowdhary et al., 2019). The ChIP DNA template was quantified by qPCR (7900HT Fast Real Time PCR

System, Applied Biosystems). A standard curve was generated using genomic DNA and ChIP DNA quantities were deduced by interpolation. The qPCR signal for each primer combination was normalized relative to the corresponding signal arising from the input DNA. Primers used in ChIP analysis are listed in **Supplemental File 1 – Table 5**.

Taq I chromosome conformation capture (Taq I-3C)

TaqI-3C was performed as previously described (Rubio & Gross, 2023). A master cell culture was grown at 30°C in YPDA from OD_{600}=0.15 to a final OD_{600}=0.8. Aliquots of 50 mL were used for each condition. Heat shock and ethanol stress were conducted as described above. Primers for analysis of 3C templates are listed in **Supplemental File 1 – Table 6**.

Fluorescence Microscopy

Widefield Fluorescence Microscopy

For **Figure 7 – figure supplement 1 [B, C]** and **Figure 8**, cells were grown at 30°C in Synthetic Complete Dextrose (SDC) medium supplemented with 0.1 mg/mL adenine to early log phase. From this culture, 90 µL were removed and cells were immobilized onto a concanavalin A (ConA, Sigma Aldrich, 100 µg/mL in ddH_2O)-coated coverslip for 20 min. The medium was then removed and replaced by either SDC or SDC + 8.5% v/v ethanol. The coverslip was mounted onto a concave microscope slide to reduce media evaporation (2-Well Concavity Slide, Electron Microscopy Sciences). Images were acquired using an AX70 Olympus epifluorescence microscope across 11 z-planes with 0.5 µm of interplanar distance. Filter set 89021 (Chroma Technology) and a Photometrics Prime 95B camera were used to image GFP and mCherry. SlideBook Software version 6.0.15 (Intelligent Imaging Innovations) was used for image capturing and z-axis stepping motor operation (Ludl Electronic products).

For heat shock, No Stress (NS) control images were taken using an Olympus Ach 100/1.25-NA objective coupled to a heating device (Bioptechs objective heater system). Heat-shocked sample imaging was done by rotating the objective away from the coverslip, switching the heating system on, and allowing it to reach 38°C before

returning the objective to the coverslip for an instantaneous heat shock. The same field of view on the coverslip was imaged for both NS and HS timepoints. For ethanol stress, an Olympus UPlanFl 100/1.4-NA objective was used for image acquisition. Analysis of the images after acquisition was done using ImageJ (v. 1.52).

In the *HSP104-TMA10* coalescence analysis, cells in which the fluorophore-tagged genes had undergone replication (two green or two red fluorescent spots, indicative of late S/G2 phase) were excluded from the analysis. The locations of the two tagged loci were analyzed over 11 different z-planes, encompassing the whole nucleus. Cells were deemed coalescence positive if they displayed colocalized, non-resolvable fluorophore signals with a distance of <0.4 µm between centroids.

Spinning Disk Confocal Microscopy

For all other imaging, cells were grown as described above and image acquisition was done using an UPlan Apo 100x/1.50 NA objective in an Olympus Yokogawa CSU W1 Spinning Disk Confocal System coupled to sCMOS cameras (Hamamatsu Fusion) controlled by cellSens Dimension software. A 50 µm pinhole disk was used for imaging in combination with 10% of laser power employed for excitation using 405 nm, 488 nm, and 561 nm lasers. Z-stacks were captured as for widefield fluorescence. For heat shock, cells were attached to a VAHEAT substrate (Interherence GmbH, Germany) (Icha et al., 2022) using ConA as above. The substrate was mounted onto the VAHEAT holder and control images were captured before heat was applied. Samples were instantaneously heated to 39° or 42°C. The substrate reservoir was covered with a coverslip to prevent media evaporation. Imaging was done over multiple timepoints as indicated in the figures. For ethanol stress, cells were mounted onto a coverslip as above, petroleum jelly was used to hold the coverslip against the concave slide and to reduce media evaporation. The slide was inverted and placed on the stage for visualization at room temperature.

Image reconstruction and analysis was done using FIJI/ImageJ (v. 1.53t) (Schindelin et al., 2012). Hsp104-BFP (LRY033) and Hsf1-mNeonGreen (LRY040) foci count and

volume were performed using the “Cells” feature in Imaris v.10.0.0. The background fluorescence was used to delimit the region of interest (ROI). This ROI was then used to quantify the number of foci per cell. For Hsp104, the ROI (whole cell) was delimited to volumes between 20 and 140 μm^3 (Uchida et al., 2011). Foci size was measured to an average of 0.4 μm in diameter, which was used to train Imaris to recognize foci of distinct sizes [“Different Spot Sizes (Region Growing)” option]. A similar approach was taken to identify the nucleus (as the cell) and the Hsf1 foci (as nucleus) using the “Cells” feature in Imaris. Nuclei with volume of 10 μm^3 ±3.7 μm^3 were used for the analysis (Larson et al., 2011). Data obtained from these analyses were plotted using GraphPad Prism 8. Plot profile for signal arising from Hsf1-mNeonGreen, Sis1-mKate, and Hsp104-BFP was done using ImageJ/FIJI.

For analysis of transcription in VPY705, *24xMS2-HSP104* mRNA was visualized using the signal arising from MCP-mCherry binding to the chimeric transcript. Cells were interrogated for transcription by assaying the presence of an mCherry focus adjacent to *HSP104-LacO*$_{256}$ bound by LacI-GFP. The high background signal from MCP-mCherry made it difficult to assess the localization of transcripts once they dissociated from the *HSP104*-tagged gene.

Statistical Tests

The statistical significance of the differences in mean values for a variety of assays was determined as specified in the figure legends using GraphPad Prism 8.

Acknowledgments

We thank Drs. Kelly Tatchell, Lucy C. Robinson, Rini Ravindran, Eric First, Surabhi Chowdhary and David Pincus for helpful discussions and technical advice; Drs. Vickky Pandit and Amoldeep Kainth for strain construction; Paula Polk for help with quantitative PCR; and Drs. Donna and Jason Brickner, Surabhi Chowdhary, Amoldeep Kainth and David Pincus for generously providing yeast strains. This work was supported by NIH grants R15 GM128065 and R01 GM138988 awarded to D.S.G. and an Ike Muslow predoctoral fellowship awarded to L.S.R.

Author Contributions

Linda S. Rubio, Conceptualization, Investigation, Visualization, Methodology, Formal Analysis, Writing – original draft, Writing – review and editing; Suman Mohajan, Investigation, Visualization, Methodology, Formal Analysis; David S. Gross, Conceptualization, Resources, Visualization, Validation, Supervision, Funding Acquisition, Writing – original draft, Writing – review and editing.

References

Albert, B., Kos-Braun, I. C., Henras, A. K., Dez, C., Rueda, M. P., Zhang, X., Gadal, O., Kos, M., & Shore, D. (2019). A ribosome assembly stress response regulates transcription to maintain proteome homeostasis. *ELife*, *8*. https://doi.org/10.7554/eLife.45002

Alberti, S., Gladfelter, A., & Mittag, T. (2019). Considerations and Challenges in Studying Liquid-Liquid Phase Separation and Biomolecular Condensates. *Cell*, *176*(3), 419–434. https://doi.org/10.1016/j.cell.2018.12.035

Ali, A., Garde, R., Schaffer, O. C., Bard, J. A. M., Husain, K., Kik, S. K., Davis, K. A., Luengo-Woods, S., Igarashi, M. G., Drummond, D. A., Squires, A. H., & Pincus, D. (2023). Adaptive preservation of orphan ribosomal proteins in chaperone-dispersed condensates. *Nature Cell Biology*, *25*(11), 1691–1703. https://doi.org/10.1038/s41556-023-01253-2

Altamirano, C. D., Kang, M., Jordan, M. A., Honigmann, A., & Franzmann, T. M. (2024). eIF4F is a thermo-sensing regulatory node in the translational heat shock response. *Molecular Cell*, *84*, 1–15. https://doi.org/10.1016/j.molcel.2024.02.038

Ansari, A., & Hampsey, M. (2005). A role for the CPF 3′ -end processing machinery in RNAP II-dependent gene looping. *Genes and Development*, *19*(24), 2969–2978. https://doi.org/10.1101/gad.1362305

Banani, S. F., Lee, H. O., Hyman, A. A., & Rosen, M. K. (2017). Biomolecular condensates: Organizers of cellular biochemistry. *Nature Reviews Molecular Cell Biology*, *18*(5), 285–298. https://doi.org/10.1038/nrm.2017.7

Bandas, E. L., & Zakharov, I. A. (1980). Induction of rho- mutations in yeast Saccharomyces cerevisiae by ethanol. *Mutation Research*, *71*(2), 193–199. https://doi.org/10.1016/0027-5107(80)90070-6

Boija, A., Klein, I. A., Sabari, B. R., Dall'Agnese, A., Coffey, E. L., Zamudio, A. V., Li, C. H., Shrinivas, K., Manteiga, J. C., Hannett, N. M., Abraham, B. J., Afeyan, L. K., Guo, Y. E., Rimel, J. K., Fant, C. B., Schuijers, J., Lee, T. I., Taatjes, D. J., & Young, R. A. (2018). Transcription Factors Activate Genes through the Phase-Separation Capacity of Their Activation Domains. *Cell*, *175*(7), 1842-1855.e16. https://doi.org/10.1016/j.cell.2018.10.042

Botman, D., de Groot, D. H., Schmidt, P., Goedhart, J., & Teusink, B. (2019). In vivo characterisation of fluorescent proteins in budding yeast. *Scientific Reports*, *9*(1). https://doi.org/10.1038/s41598-019-38913-z

Bradley, A. I., Marsh, N. M., Borror, H. R., Mostoller, K. E., Gama, A. I., & Gardner, R. G. (2021). Acute ethanol stress induces sumoylation of conserved chromatin structural proteins in Saccharomyces cerevisiae. *Molecular Biology of the Cell*, *32*, 1121–1133. https://doi.org/10.1091/mbc.e20-11-0715

Breeden, L. L., & Tsukiyama, T. (2022). Quiescence in Saccharomyces cerevisiae. *Annual Review of Genetics*, *56*, 253–278. https://doi.org/10.1146/annurev-genet-080320-023632

Bresson, S., Shchepachev, V., Spanos, C., Turowski, T. W., Rappsilber, J., & Tollervey, D. (2020). Stress-Induced Translation Inhibition through Rapid Displacement of Scanning Initiation Factors. *Molecular Cell*, *80*(0).

https://doi.org/10.1016/j.molcel.2020.09.021
Brickner, D. G., Randise-Hinchliff, C., Corbin, M. L., Liang, J. M., Kim, S., Sump, B., D'Urso, A., Kim, S. H., Satomura, A., Schmit, H., Coukos, R., Hwang, S., Watson, R., & Brickner, J. H. (2019). The Role of Transcription Factors and Nuclear Pore Proteins in Controlling the Spatial Organization of the Yeast Genome. *Developmental Cell*, *49*(6), 936-947.e4. https://doi.org/10.1016/j.devcel.2019.05.023
Brickner, J. H., & Walter, P. (2004). Gene recruitment of the activated INO1 locus to the nuclear membrane. *PLoS Biology*, *2*(11), e342. https://doi.org/10.1371/journal.pbio.0020342
Brodsky, S., Jana, T., Mittelman, K., Chapal, M., Kumar, D. K., Carmi, M., & Barkai, N. (2020). Intrinsically Disordered Regions Direct Transcription Factor In Vivo Binding Specificity. *Molecular Cell*, *79*(3), 459-471.e4. https://doi.org/10.1016/j.molcel.2020.05.032
Cabal, G. G., Genovesio, A., Rodriguez-Navarro, S., Zimmer, C., Gadal, O., Lesne, A., Buc, H., Feuerbach-Fournier, F., Olivo-Marin, J. C., Hurt, E. C., & Nehrbass, U. (2006). SAGA interacting factors confine sub-diffusion of transcribed genes to the nuclear envelope. *Nature*, *441*(7094), 770–773. https://doi.org/10.1038/nature04752
Casolari, J. M., Brown, C. R., Komili, S., West, J., Hieronymus, H., & Silver, P. A. (2004). Genome-wide localization of the nuclear transport machinery couples transcriptional status and nuclear organization. *Cell*, *117*(4), 427–439. https://doi.org/10.1016/S0092-8674(04)00448-9
Cho, W. K., Spille, J. H., Hecht, M., Lee, C., Li, C., Grube, V., & Cisse, I. I. (2018). Mediator and RNA polymerase II clusters associate in transcription-dependent condensates. *Science*, *361*(6400), 412–415. https://doi.org/10.1126/science.aar4199
Chowdhary, S., Kainth, A. S., & Gross, D. S. (2017). Heat Shock Protein Genes Undergo Dynamic Alteration in Their Three-Dimensional Structure and Genome Organization in Response to Thermal Stress. *Molecular and Cellular Biology*, *37*(24), 1–23. https://doi.org/10.1128/mcb.00292-17
Chowdhary, S., Kainth, A. S., & Gross, D. S. (2020). Chromosome conformation capture that detects novel cis- and trans-interactions in budding yeast. *Methods*, *170*, 4–16. https://doi.org/10.1016/j.ymeth.2019.06.023
Chowdhary, S., Kainth, A. S., Paracha, S., Gross, D. S., & Pincus, D. (2022). Inducible transcriptional condensates drive 3D genome reorganization in the heat shock response. *Molecular Cell*, *82*(22), 4386-4399.e7. https://doi.org/10.1016/j.molcel.2022.10.013
Chowdhary, S., Kainth, A. S., Pincus, D., & Gross, D. S. (2019). Heat Shock Factor 1 Drives Intergenic Association of Its Target Gene Loci upon Heat Shock. *Cell Reports*, *26*(1), 18-28.e5. https://doi.org/10.1016/j.celrep.2018.12.034
Costa, V., Amorim, M. A., Reis, E., Quintanilha, A., & Moradas-Ferreira, P. (1997). Mitochondrial superoxide dismutase is essential for ethanol tolerance of Saccharomyces cerevisiae in the post-diauxic phase. *Microbiology*, *143*(5), 1649–1656. https://doi.org/10.1099/00221287-143-5-1649
Dashko, S., Zhou, N., Compagno, C., & Piškur, J. (2014). Why, when, and how did

yeast evolve alcoholic fermentation? *FEMS Yeast Research*, *14*(6), 826–832. https://doi.org/10.1111/1567-1364.12161

Davidson, J. F., & Schiestl, R. H. (2001). Mitochondrial Respiratory Electron Carriers Are Involved in Oxidative Stress during Heat Stress in Saccharomyces cerevisiae . *Molecular and Cellular Biology*, *21*(24), 8483–8489. https://doi.org/10.1128/mcb.21.24.8483-8489.2001

Davidson, J. F., Whyte, B., Bissinger, P. H., & Schiestl, R. H. (1996). Oxidative stress is involved in heat-induced cell death in Saccharomyces cerevisiae. *Proceedings of the National Academy of Sciences of the United States of America*, *93*(10), 5116–5121. https://doi.org/10.1073/pnas.93.10.5116

Dieppois, G., Iglesias, N., & Stutz, F. (2006). Cotranscriptional Recruitment to the mRNA Export Receptor Mex67p Contributes to Nuclear Pore Anchoring of Activated Genes. *Molecular and Cellular Biology*, *26*(21), 7858–7870. https://doi.org/10.1128/mcb.00870-06

Du, M., Zhang, Q., & Bai, L. (2017). Three distinct mechanisms of long-distance modulation of gene expression in yeast. *PLoS Genetics*, *13*(4), e1006736. https://doi.org/10.1371/journal.pgen.1006736

Duan, Z., Andronescu, M., Schutz, K., McIlwain, S., Kim, Y. J., Lee, C., Shendure, J., Fields, S., Blau, C. A., & Noble, W. S. (2010). A three-dimensional model of the yeast genome. *Nature*, *465*(7296), 363–367. https://doi.org/10.1038/nature08973

Erkine, A. M., Adams, C. C., Diken, T., & Gross, D. S. (1996). Heat shock factor gains access to the yeast HSC82 promoter independently of other sequence-specific factors and antagonizes nucleosomal repression of basal and induced transcription. *Molecular and Cellular Biology*, *16*(12), 7004–7017.

Eser, U., Chandler-Brown, D., Ay, F., Straight, A. F., Duan, Z., Noble, W. S., & Skotheim, J. M. (2017). Form and function of topologically associating genomic domains in budding yeast. *Proceedings of the National Academy of Sciences of the United States of America*, *114*(15), E3061–E3070. https://doi.org/10.1073/pnas.1612256114

Fanucchi, S., Shibayama, Y., Burd, S., Weinberg, M. S., & Mhlanga, M. M. (2013). Chromosomal contact permits transcription between coregulated genes. *Cell*, *155*(3), 606. https://doi.org/10.1016/J.CELL.2013.09.051

Feder, Z. A., Ali, A., Singh, A., Krakowiak, J., Zheng, X., Bindokas, V. P., Wolfgeher, D., Kron, S. J., & Pincus, D. (2021). Subcellular localization of the J-protein Sis1 regulates the heat shock response. *Journal of Cell Biology*, *220*(1), e202005165. https://doi.org/10.1083/JCB.202005165

Furutani, N., & Izawa, S. (2022). Adaptability of wine yeast to ethanol-induced protein denaturation. *FEMS Yeast Research*, *22*(1), 1–8. https://doi.org/10.1093/femsyr/foac059

Gaglia, G., Rashid, R., Yapp, C., Joshi, G. N., Li, C. G., Lindquist, S. L., Sarosiek, K. A., Whitesell, L., Sorger, P. K., & Santagata, S. (2020). HSF1 phase transition mediates stress adaptation and cell fate decisions. *Nature Cell Biology*, *22*(2), 151–158. https://doi.org/10.1038/s41556-019-0458-3

Gasch, A. P., Spellman, P. T., Kao, C. M., Carmel-Harel, O., Eisen, M. B., Storz, G., Botstein, D., & Brown, P. O. (2000). Genomic expression programs in the response of yeast cells to environmental changes. *Molecular Biology of the Cell*, *11*(12),

4241–4257. https://doi.org/10.1091/mbc.11.12.4241
Giardina, C., & Lis, J. T. (1995). Dynamic protein-DNA architecture of a yeast heat shock promoter. *Molecular and Cellular Biology*, *15*(5), 2737–2744. https://doi.org/10.1128/mcb.15.5.2737
Green, E. M., Jiang, Y., Joyner, R., & Weis, K. (2012). A negative feedback loop at the nuclear periphery regulates GAL gene expression. *Molecular Biology of the Cell*, *23*(7), 1367–1375. https://doi.org/10.1091/mbc.E11-06-0547
Grouši, T., Ivanov, P., Frýdlová, I., Vašicová, P., Janda, F., Vojtová, J., Malínská, K., Malcová, I., Nováková, L., Janošková, D., Valášek, L., & Hašek, J. (2009). Robust heat shock induces eIF2α-phosphorylationin-dependent assembly of stress granules containing eIF3 and 40S ribosomal subunits in budding yeast, Saccharomyces cerevisiae. *Journal of Cell Science*, *122*(12), 2078–2088. https://doi.org/10.1242/jcs.045104
Haim, L., Zipor, G., Aronov, S., & Gerst, J. E. (2007). A genomic integration method to visualize localization of endogenous mRNAs in living yeast. *Nature Methods*, *4*(5), 409–412. https://doi.org/10.1038/nmeth1040
Herman, P. K. (2002). Stationary phase in yeast. *Current Opinion in Microbiology*, *5*(6), 602–607. https://doi.org/10.1016/S1369-5274(02)00377-6
Hnisz, D., Shrinivas, K., Young, R. A., Chakraborty, A. K., & Sharp, P. A. (2017). A Phase Separation Model for Transcriptional Control. *Cell*, *169*(1), 13–23. https://doi.org/10.1016/j.cell.2017.02.007
Homoto, S., & Izawa, S. (2018). Persistent actin depolarization caused by ethanol induces the formation of multiple small cortical septin rings in yeast. *Journal of Cell Science*, *131*(15). https://doi.org/10.1242/jcs.217091
Hsieh, T. H. S., Weiner, A., Lajoie, B., Dekker, J., Friedman, N., & Rando, O. J. (2015). Mapping Nucleosome Resolution Chromosome Folding in Yeast by Micro-C. *Cell*, *162*(1), 108–119. https://doi.org/10.1016/j.cell.2015.05.048
Icha, J., Böning, D., & Türschmann, P. (2022). Precise and Dynamic Temperature Control in High-Resolution Microscopy with VAHEAT. *Microscopy Today*, *30*(1), 34–41. https://doi.org/10.1017/s1551929521001553
Itoh, Y., Iida, S., Tamura, S., Nagashima, R., Shiraki, K., Goto, T., Hibino, K., Ide, S., & Maeshima, K. (2021). 1,6-hexanediol rapidly immobilizes and condenses chromatin in living human cells. *Life Science Alliance*, *4*(4). https://doi.org/10.26508/LSA.202001005
Izawa, S., Kita, T., Ikeda, K., & Inoue, Y. (2008). Heat shock and ethanol stress provoke distinctly different responses in 3′-processing and nuclear export of HSP mRNA in Saccharomyces cerevisiae. *Biochemical Journal*, *414*(1), 111–119. https://doi.org/10.1042/BJ20071567
Johnston, G. C., & Singer, R. A. (1980). Ribosomal precursor RNA metabolism and cell division in the yeast Saccharomyces cerevisiae. *Molecular & General Genetics*, *178*(2), 357–360. https://doi.org/10.1007/BF00270484
Jolly, C., Konecny, L., Grady, D. L., Kutskova, Y. A., Cotto, J. J., Morimoto, R. I., & Vourc'h, C. (2002). In vivo binding of active heat shock transcription factor 1 to human chromosome 9 heterochromatin during stress. *Journal of Cell Biology*, *156*(5), 775–781. https://doi.org/10.1083/jcb.200109018
Jolly, C., Morimoto, R. I., Robert-Nicoud, M., & Vourc'h, C. (1997). HSF1 transcription

factor concentrates in nuclear foci during heat shock: Relationship with transcription sites. *Journal of Cell Science*, *110*(23), 2935–2941. https://doi.org/10.1242/jcs.110.23.2935

Kato, K., Yamamoto, Y., & Izawa, S. (2011). Severe ethanol stress induces assembly of stress granules in Saccharomyces cerevisiae. *Yeast*, *28*(5), 339–347. https://doi.org/10.1002/yea.1842

Kato, S., Yoshida, M., & Izawa, S. (2019). Btn2 is involved in the clearance of denatured proteins caused by severe ethanol stress in Saccharomyces cerevisiae. *FEMS Yeast Research*, *19*(8), 1–8. https://doi.org/10.1093/femsyr/foz079

Kim, S., & Gross, D. S. (2013). Mediator recruitment to heat shock genes requires dual Hsf1 activation domains and Mediator tail subunits Med15 and Med16. *Journal of Biological Chemistry*, *288*(17), 12197–12213. https://doi.org/10.1074/jbc.M112.449553

Krakowiak, J., Zheng, X., Patel, N., Feder, Z. A., Anandhakumar, J., Valerius, K., Gross, D. S., Khalil, A. S., & Pincus, D. (2018). Hsf1 and Hsp70 constitute a two-component feedback loop that regulates the yeast heat shock response. *ELife*, *7*, 1–17. https://doi.org/10.7554/eLife.31668

Kremer, S. B., & Gross, D. S. (2009). SAGA and Rpd3 chromatin modification complexes dynamically regulate heat shock gene structure and expression. *Journal of Biological Chemistry*, *284*(47), 32914–32931.

Kubota, S., Takeo, I., Kume, K., Kanai, M., Shitamukai, A., Mizunuma, M., Miyakawa, T., Shimoi, H., Iefuji, H., & Hirata, D. (2004). Effect of ethanol on cell growth of budding yeast: Genes that are important for cell growth in the presence of ethanol. *Bioscience, Biotechnology and Biochemistry*, *68*(4), 968–972. https://doi.org/10.1271/bbb.68.968

Larson, D. R., Zenklusen, D., Wu, B., Chao, J. A., & Singer, R. H. (2011). Real-time observation of transcription initiation and elongation on an endogenous yeast gene. *Science*, *332*(6028), 475–478. https://doi.org/10.1126/science.1202142

Lee, J., Simpson, L., Li, Y., Becker, S., Zou, F., Zhang, X., & Bai, L. (2024). Transcription Factor Condensates Mediate Clustering of MET Regulon and Enhancement in Gene Expression. *BioRxiv*. https://doi.org/10.1101/2024.02.06.579062

Lee, M. S., & Garrard, W. T. (1991). Transcription-induced nucleosome “splitting”: An underlying structure for DNase I sensitive chromatin. *EMBO Journal*, *10*(3), 607–615. https://doi.org/10.1002/j.1460-2075.1991.tb07988.x

Liti, G. (2015). The fascinating and secret wild life of the budding yeast S. cerevisiae. *ELife*, *4*. https://doi.org/10.7554/eLife.05835

Liu, B., Larsson, L., Caballero, A., Hao, X., Öling, D., Grantham, J., & Nyström, T. (2010). The Polarisome Is Required for Segregation and Retrograde Transport of Protein Aggregates. *Cell*, *140*(2), 257–267. https://doi.org/10.1016/j.cell.2009.12.031

McMurry, J. (2012). *Organic Chemistry* (L. Lockwood, S. Kiselica, & E. Woods (eds.); 8th ed.). Brooks/Cole.

Meduri, R., Rubio, L. S., Mohajan, S., & Gross, D. S. (2022). Phase-separation antagonists potently inhibit transcription and broadly increase nucleosome density. *Journal of Biological Chemistry*, *298*(10), 102365.

https://doi.org/10.1016/j.jbc.2022.102365
Meeussen, J. V. W., Pomp, W., Brouwer, I., De Jonge, W. J., Patel, H. P., & Lenstra, T. L. (2023). Transcription factor clusters enable target search but do not contribute to target gene activation. *Nucleic Acids Research*, *51*(11), 5449–5468. https://doi.org/10.1093/nar/gkad227
Monahan, K., & Lomvardas, S. (2015). Monoallelic Expression of Olfactory Receptors. *Annual Review of Cell and Developmental Biology*, *31*, 721–740. https://doi.org/10.1146/annurev-cellbio-100814-125308
Morawska, M., & Ulrich, H. D. (2013). An expanded tool kit for the auxin-inducible degron system in budding yeast. *Yeast*, *30*(9), 341–351. https://doi.org/10.1002/yea.2967
Nair, S. J., Yang, L., Meluzzi, D., Oh, S., Yang, F., Friedman, M. J., Wang, S., Suter, T., Alshareedah, I., Gamliel, A., Ma, Q., Zhang, J., Hu, Y., Tan, Y., Ohgi, K. A., Jayani, R. S., Banerjee, P. R., Aggarwal, A. K., & Rosenfeld, M. G. (2019). Phase separation of ligand-activated enhancers licenses cooperative chromosomal enhancer assembly. *Nature Structural and Molecular Biology*, *26*(3), 193–203. https://doi.org/10.1038/s41594-019-0190-5
O'Sullivan, J. M., Tan-Wong, S. M., Morillon, A., Lee, B., Coles, J., Mellor, J., & Proudfoot, N. J. (2004). Gene loops juxtapose promoters and terminators in yeast. *Nature Genetics*, *36*(9), 1014–1018.
Papantonis, A., Kohro, T., Baboo, S., Larkin, J. D., Deng, B., Short, P., Tsutsumi, S., Taylor, S., Kanki, Y., Kobayashi, M., Li, G., Poh, H. M., Ruan, X., Aburatani, H., Ruan, Y., Kodama, T., Wada, Y., & Cook, P. R. (2012). TNFα signals through specialized factories where responsive coding and miRNA genes are transcribed. *EMBO Journal*, *31*(23), 4404–4414. https://doi.org/10.1038/emboj.2012.288
Park, S. K., Xiang, Y., Feng, X., & Garrard, W. T. (2014). Pronounced cohabitation of active immunoglobulin genes from three different chromosomes in transcription factories during maximal antibody synthesis. *Genes and Development*, *28*(11), 1159–1164. https://doi.org/10.1101/gad.237479.114
Peffer, S., Gonçalves, D., & Morano, K. A. (2019). Regulation of the Hsf1-dependent transcriptome via conserved bipartite contacts with Hsp70 promotes survival in yeast. *Journal of Biological Chemistry*, *294*(32), 12191–12202.
Pincus, D., Anandhakumar, J., Thiru, P., Guertin, M. J., Erkine, A. M., & Gross, D. S. (2018). Genetic and epigenetic determinants establish a continuum of Hsf1 occupancy and activity across the yeast genome. *Molecular Biology of the Cell*, *29*(26), 3168–3182. https://doi.org/10.1091/mbc.E18-06-0353
Piper, P. W. (1995). The heat shock and ethanol stress responses of yeast exhibit extensive similarity and functional overlap. *FEMS Microbiology Letters*, *134*(2–3), 121–127. doi:10.1111/j.1574-6968.1995.tb07925.x
Piper, P. W., Talreja, K., Panaretou, B., Moradas-Ferreira, P., Byrne, K., Praekelt, U. M., Meacock, P., Recnacq, M., & Boucherie, H. (1994). Induction of major heat-shock proteins of Saccharomyces cerevisiae, including plasma membrane Hsp30, by ethanol levels above a critical threshold. *Microbiology*, *140*(11), 3031–3038. https://doi.org/10.1099/13500872-140-11-3031
Piškur, J., Rozpedowska, E., Polakova, S., Merico, A., & Compagno, C. (2006). How did Saccharomyces evolve to become a good brewer? *Trends in Genetics*, *22*(4), 183–

186. https://doi.org/10.1016/j.tig.2006.02.002
Plesset, J., Palm, C., & McLaughlin, C. S. (1982). Induction of heat shock proteins and thermotolerance by ethanol in Saccharomyces cerevisiae. *Biochemical and Biophysical Research Communications*, *108*(3), 1340–1345. https://doi.org/10.1016/0006-291X(82)92147-7
Rosa, M. F., & Sá-Correia, I. (1991). In vivo activation by ethanol of plasma membrane ATPase of Saccharomyces cerevisiae. *Applied and Environmental Microbiology*, *57*(3), 830–835. https://doi.org/10.1128/aem.57.3.830-835.1991
Rosa, M. F., & Sá-Correia, I. (1996). Intracellular acidification does not account for inhibition of Saccharomyces cerevisiae growth in the presence of ethanol. *FEMS Microbiology Letters*, *135*(2–3), 271–274. doi: 10.1111/j.1574-6968.1996.tb08000.x
Rozpedowska, E., Hellborg, L., Ishchuk, O. P., Orhan, F., Galafassi, S., Merico, A., Woolfit, M., Compagno, C., & Piškur, J. (2011). Parallel evolution of the make-accumulate-consume strategy in Saccharomyces and Dekkera yeasts. *Nature Communications*, *2*(1), 1–7. https://doi.org/10.1038/ncomms1305
Rubio, L. S., & Gross, D. S. (2023). Dynamic coalescence of yeast Heat Shock Protein genes bypasses the requirement for actin. *Genetics*, *223*(4). https://doi.org/10.1093/genetics/iyad006
Sabari, B. R., Dall'Agnese, A., Boija, A., Klein, I. A., Coffey, E. L., Shrinivas, K., Abraham, B. J., Hannett, N. M., Zamudio, A. V., Manteiga, J. C., Li, C. H., Guo, Y. E., Day, D. S., Schuijers, J., Vasile, E., Malik, S., Hnisz, D., Lee, T. I., Cisse, I. I., … Young, R. A. (2018). Coactivator condensation at super-enhancers links phase separation and gene control. *Science*, *361*(6400), eaar3958. https://doi.org/10.1126/science.aap9195
Schindelin, J., Arganda-Carreras, I., Frise, E., Kaynig, V., Longair, M., Pietzsch, T., Preibisch, S., Rueden, C., Saalfeld, S., Schmid, B., Tinevez, J. Y., White, D. J., Hartenstein, V., Eliceiri, K., Tomancak, P., & Cardona, A. (2012). Fiji: An open-source platform for biological-image analysis. *Nature Methods*, *9*(7), 676–682. https://doi.org/10.1038/nmeth.2019
Schoenfelder, S., Sexton, T., Chakalova, L., Cope, N. F., Horton, A., Andrews, S., Kurukuti, S., Mitchell, J. A., Umlauf, D., Dimitrova, D. S., Eskiw, C. H., Luo, Y., Wei, C. L., Ruan, Y., Bieker, J. J., & Fraser, P. (2010). Preferential associations between co-regulated genes reveal a transcriptional interactome in erythroid cells. *Nature Genetics*, *42*(1), 53–61. https://doi.org/10.1038/ng.496
Schulz, K. N., & Harrison, M. M. (2019). Mechanisms regulating zygotic genome activation. *Nature Reviews Genetics*, *20*(4), 221–234. https://doi.org/10.1038/s41576-018-0087-x
Sekinger, E. A., & Gross, D. S. (2001). Silenced chromatin is permissive to activator binding and PIC recruitment. *Cell*, *105*(3), 403–414.
Shaner, N. C., Lambert, G. G., Chammas, A., Ni, Y., Cranfill, P. J., Baird, M. A., Sell, B. R., Allen, J. R., Day, R. N., Israelsson, M., Davidson, M. W., & Wang, J. (2013). A bright monomeric green fluorescent protein derived from Branchiostoma lanceolatum. *Nature Methods*, *10*(5), 407–409. https://doi.org/10.1038/nmeth.2413
Shen, L., Wang, Y. T., Tang, X. X., Zhang, K., Wang, P. M., Sui, Y., & Zheng, D. Q. (2020). Heat shock drives genomic instability and phenotypic variations in yeast. *AMB Express*, *10*(1). https://doi.org/10.1186/s13568-020-01091-7

Stanley, D., Bandara, A., Fraser, S., Chambers, P. J., & Stanley, G. A. (2010). The ethanol stress response and ethanol tolerance of Saccharomyces cerevisiae. *Journal of Applied Microbiology*, *109*(1), 13–24.

Taddei, A., & Gasser, S. M. (2012). Structure and function in the budding yeast nucleus. *Genetics*, *192*(1), 107–129. https://doi.org/10.1534/genetics.112.140608

Tan, J. J. D., Ma, Z., Xie, Y., Yang, L., & Miao, Y. (2017). Quantitative analysis of actin filament assembly in yeast and plant by live cell fluorescence microscopy. *Micron*, *103*, 78–83. https://doi.org/10.1016/j.micron.2017.09.011

Triandafillou, C. G., Katanski, C. D., Dinner, A. R., & Allan Drummond, D. (2020). Transient intracellular acidification regulates the core transcriptional heat shock response. *ELife*, *9*, e54880. doi: https://doi.org/10.7554/eLife.54880

Tye, B. W., & Churchman, L. S. (2021). Hsf1 activation by proteotoxic stress requires concurrent protein synthesis. *Molecular Biology of the Cell*, *32*(19), 1800–1806. https://doi.org/10.1091/mbc.E21-01-0014

Tye, B. W., Commins, N., Ryazanova, L. V., Wühr, M., Springer, M., Pincus, D., & Churchman, L. S. (2019). Proteotoxicity from aberrant ribosome biogenesis compromises cell fitness. *ELife*, *8*. https://doi.org/10.7554/eLife.43002

Uchida, M., Sun, Y., McDermott, G., Knoechel, C., Gros, M. A. Le, Parkinson, D., Drubin, D. G., & Larabell, C. A. (2011). Quantitative analysis of yeast internal architecture using soft X-ray tomography. *Yeast*, *28*, 227–236. https://doi.org/10.1002/yea.1834

Verghese, J., Abrams, J., Wang, Y., & Morano, K. A. (2012). Biology of the Heat Shock Response and Protein Chaperones: Budding Yeast (Saccharomyces cerevisiae) as a Model System. *Microbiology and Molecular Biology Reviews*, *76*(2), 115–158. https://doi.org/10.1128/mmbr.05018-11

Voordeckers, K., Colding, C., Grasso, L., Pardo, B., Hoes, L., Kominek, J., Gielens, K., Dekoster, K., Gordon, J., Van der Zande, E., Bircham, P., Swings, T., Michiels, J., Van Loo, P., Nuyts, S., Pasero, P., Lisby, M., & Verstrepen, K. J. (2020). Ethanol exposure increases mutation rate through error-prone polymerases. *Nature Communications*, *11*(1), 3664. https://doi.org/10.1038/s41467-020-17447-3

Wendt, K. S., & Grosveld, F. G. (2014). Transcription in the context of the 3D nucleus. *Current Opinion in Genetics and Development*, *25*(1), 62–67. https://doi.org/10.1016/j.gde.2013.11.020

Zander, G., Hackmann, A., Bender, L., Becker, D., Lingner, T., Salinas, G., & Krebber, H. (2016). MRNA quality control is bypassed for immediate export of stress-responsive transcripts. *Nature*, *540*(7634), 593–596. https://doi.org/10.1038/nature20572

Zhang, H., Gao, L., Anandhakumar, J., & Gross, D. S. (2014). Uncoupling Transcription from Covalent Histone Modification. *PLoS Genetics*, *10*(4). https://doi.org/10.1371/journal.pgen.1004202

Zhang, H., Shao, S., Zeng, Y., Wang, X., Qin, Y., Ren, Q., Xiang, S., Wang, Y., Xiao, J., & Sun, Y. (2022). Reversible phase separation of HSF1 is required for an acute transcriptional response during heat shock. *Nature Cell Biology*, *24*(3), 340–352. https://doi.org/10.1038/s41556-022-00846-7

Zhao, J., Herrera-Diaz, J., & Gross, D. S. (2005). Domain-Wide Displacement of Histones by Activated Heat Shock Factor Occurs Independently of Swi/Snf and Is

Not Correlated with RNA Polymerase II Density. *Molecular and Cellular Biology*, *25*(20), 8985–8999. https://doi.org/10.1128/mcb.25.20.8985-8999.2005

Zheng, X., Krakowiak, J., Patel, N., Beyzavi, A., Ezike, J., Khalil, A. S., & Pincus, D. (2016). Dynamic control of Hsf1 during heat shock by a chaperone switch and phosphorylation. *ELife*, *5*. https://doi.org/10.7554/eLife.18638

Tables

Table 1. Kinetics of select nuclear phenomena in response to heat shock and ethanol stress

Parameter	Heat Shock (39°C)	Ethanol Stress (8.5% v/v)
Hsf1 binding to HSEs	Rapid, peak at 2.5 min	Slight delay, peak at 10 min
Pol II recruitment to *HSRs*	Rapid, peak at 2.5 min	Severely delayed, detection starts at 10 min
Histone H3 occupancy at *HSRs*	Rapid depletion	Transient increase, followed by gradual depletion
Genome compaction[1]	Transient	Sustained
HSR gene transcription	Rapid	Delayed
HSR gene coalescence	Rapid, transient	Slightly delayed, transient
Hsf1 condensates	Rapidly induced, transient, well defined	Rapidly induced, stable, poorly defined

[1] As inferred from enhanced H3 ChIP signal at non-Hsf1 regulated loci.

Graphical Abstract

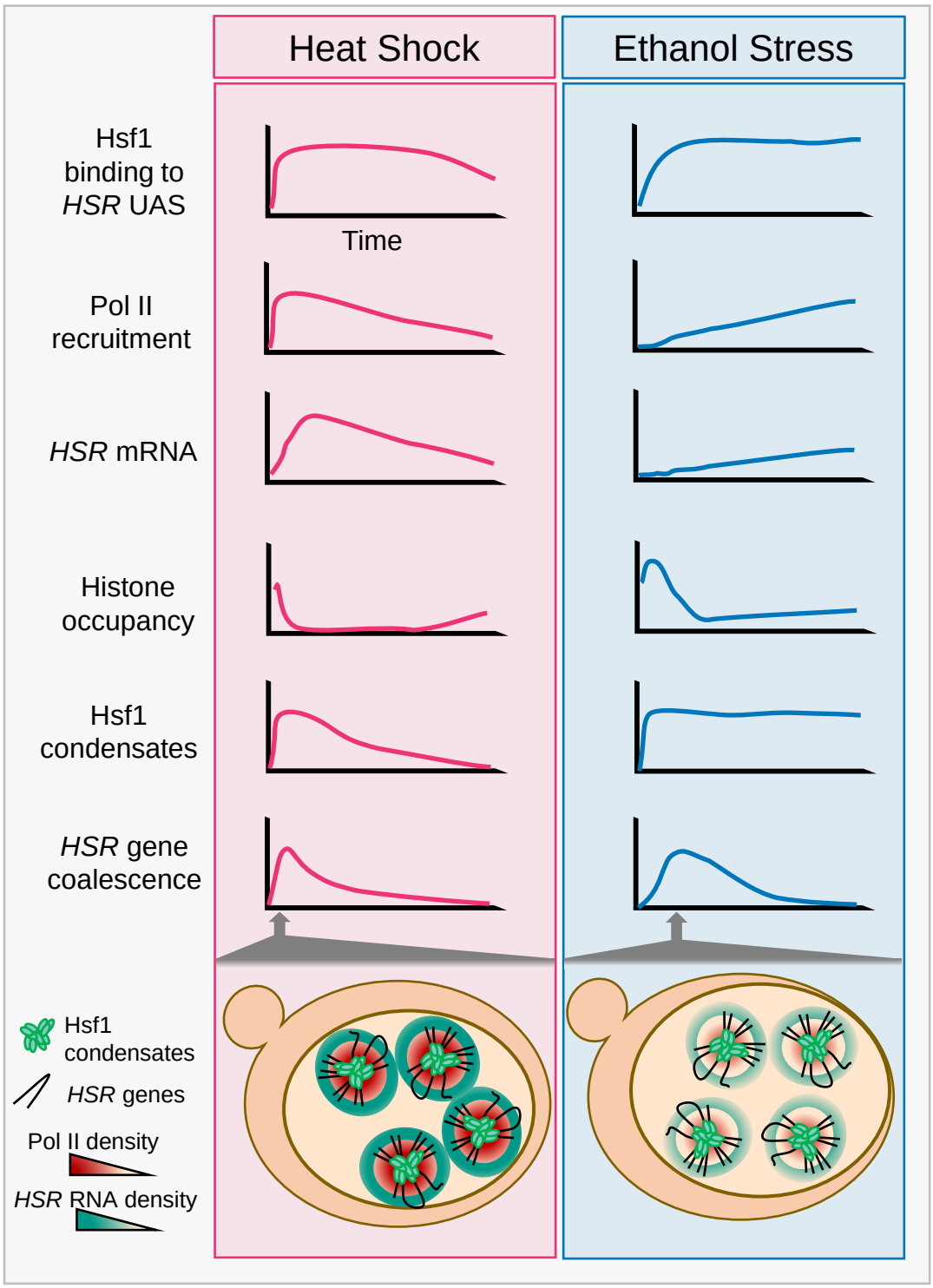

Figure 1

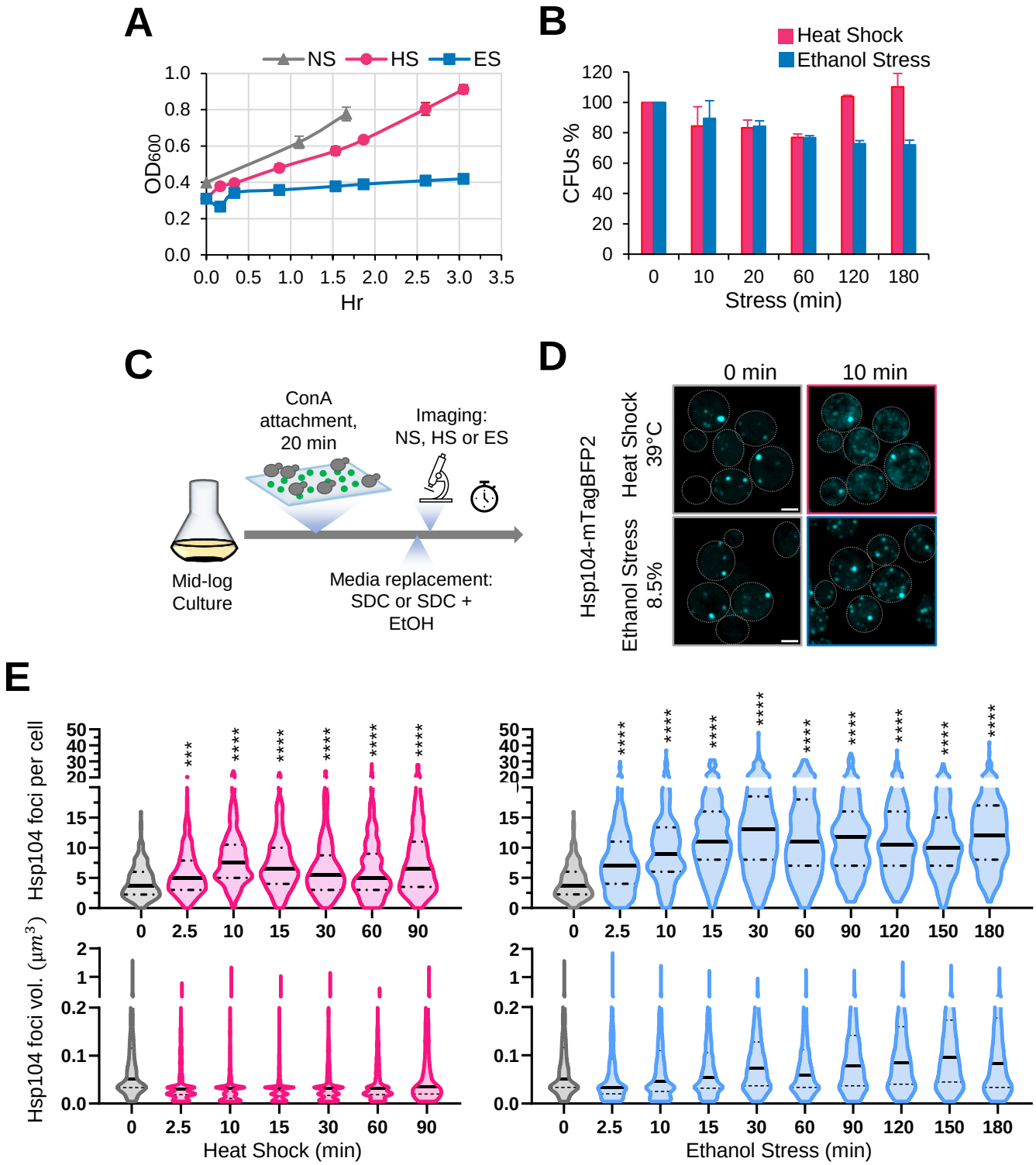
A
NS
HS
ES
OD600
Hr
B
Heat Shock
Ethanol Stress
CFUs %
Stress (min)
C
ConA attachment, 20 min
Imaging: NS, HS or ES
Mid-log Culture
Media replacement: SDC or SDC + EtOH
D
0 min
10 min
Hsp104-mTagBFP2
Heat Shock 39°C
Ethanol Stress 8.5%
E
Hsp104 foci per cell
Hsp104 foci vol. (μm³)
Heat Shock (min)
Ethanol Stress (min)

Figure 1. Thermal and chemical stresses used in this study elicit distinct proteotoxic responses.

(A) Growth curve of strain W303-1B grown in liquid culture (YPDA). Mid-log phase cultures were diluted to OD_{600}=0.4 and shifted to different conditions: no stress (NS, 25°C), heat shock (HS, 39°C), or ethanol stress (ES, 8.5% v/v, 25°C). OD_{600} was monitored over time. Means and SD are shown. N=2.

(B) Viability assay of W303-1B cells following exposure to heat shock (25° to 39°C upshift for the indicated time) or ethanol stress (8.5% v/v ethanol for the indicated time at 25°C). An aliquot was taken from each condition at the listed stress timepoints and diluted in rich media. Cells were spread on YPDA plates and grown at 30°C for 3 days. Colony forming units (CFUs) were determined using ImageJ/FIJI. Plotted are percentages of CFUs of stressed cells normalized to those of the 0 min control. Graphs depict means + SD. N=2.

(C) Experimental strategy for imaging Hsp104 foci. Cells were attached to a concanavalin A (ConA)-coated surface, followed by heat shock or ethanol stress treatment (see Materials and Methods). Synthetic complete media (SDC) was supplemented with ethanol to a final concentration of 8.5% for ES samples. Scale bar: 2 µm.

(D) Both heat shock and ethanol stress induce formation of Hsp104 foci. DPY1561 cells were attached to a VAHEAT substrate using Concanavalin A and subjected to an instantaneous heat shock (25° to 39°C) or to ethanol stress (25°C, 8.5% v/v). 0 min control was kept at 25°C without stress. Hsp104-mTagBFP2 foci were visualized by confocal microscopy. Shown are maximal projections of 11 z-planes, taken with an interplanar distance of 0.5 µm. Scale bar: 2 µm.

(E) Cells subjected to the above treatments were assayed for Hsp104 puncta number and volume. An average of 200 cells per timepoint, per condition, was quantified using Imaris image analysis software (v.10.0.1). For this analysis, we made the assumption that the diffuse Hsp104 clusters seen in HS cells are comparable to the compact Hsp104 foci in ES cells. N=2. Significance was determined by Mann Whitney test, stress (T≥2.5 min) vs. no stress. ***, $p<0.001$; ****, $p<0.0001$.

Figure 2

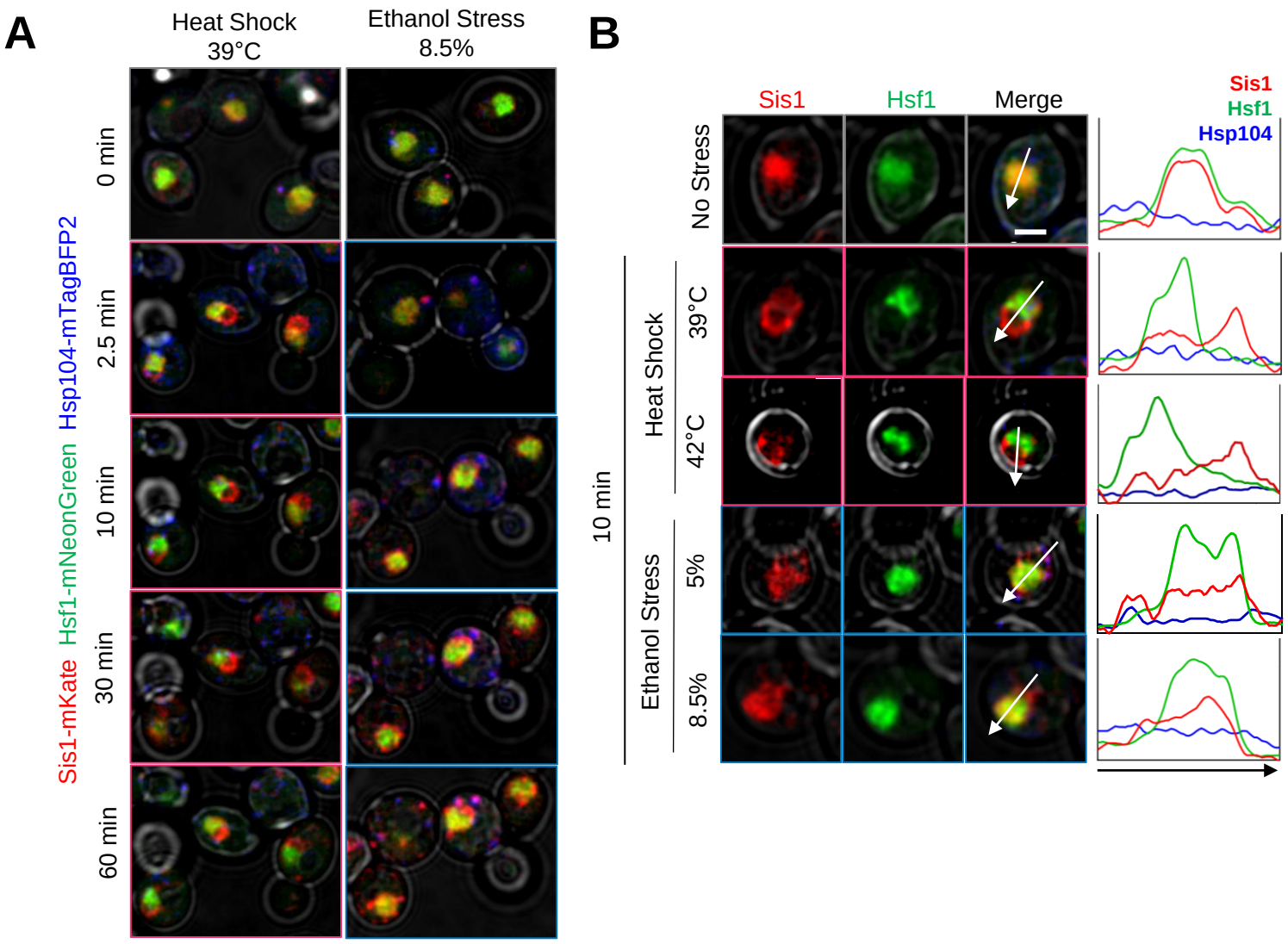

Figure 2. Heat shock and ethanol stress elicit distinct patterns of Sis1 subcellular relocalization.

(A) Live cell confocal microscopy of the diploid strain LRY033 expressing Sis1-mKate, Hsf1-mNeonGreen, and Hsp104-mTagBFP2. Cells were treated as in Figure 1D. 11 z-planes were captured with an interplanar distance of 0.5 µm. Shown is a representative plane for each timepoint.

(B) Subcellular localization analysis of Sis1, Hsf1 and Hsp104 in cells subjected to no stress (25°C), heat shock (at 39° or 42°C) or ethanol stress (at 5% or 8.5% v/v (25°C)) for 10 min. Cells from strain LRY033 were treated as described in Figure 1D. A representative plane is shown for each condition. Line profiles are plotted for each channel on the right. Arrows were drawn to bisect the nucleus. Scale bar: 2 µm.

Figure 3

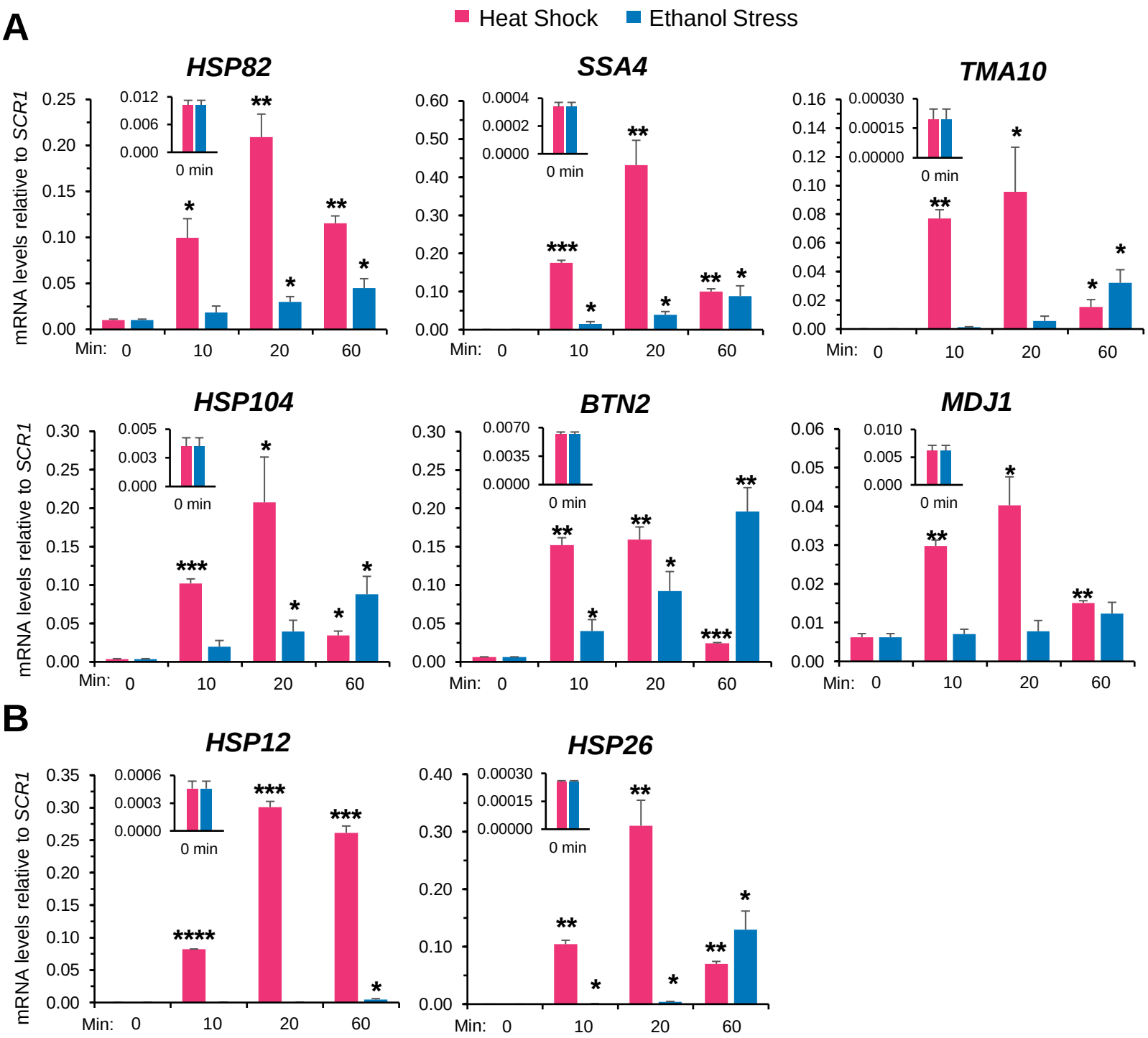

Figure 3. Ethanol stress transcriptionally induces *Heat Shock Response (HSR)* genes but with markedly slower kinetics than thermal stress.

(A) RNA abundance of Hsf1-dependent *HSR* genes was determined by Reverse Transcription-qPCR in strain W303-1B. Heat shock was performed at 39°C; ethanol stress was done using 8.5% (v/v) ethanol at 25°C. Insets display transcript abundance using a zoomed-in scale. Depicted are means + SD. N=2, qPCR=4. Statistical analysis: T-test, one-tailed, no stress vs. stress conditions. *, $p<0.05$; **, $p<0.01$, ***; $p<0.001$.

(B) As in (A), but the Hsf1-, Msn2-dual regulated genes *HSP12* and *HSP26* were evaluated. *, $p<0.05$; ***, $p<0.001$; ****, $p< 0.0001$.

Figure 4

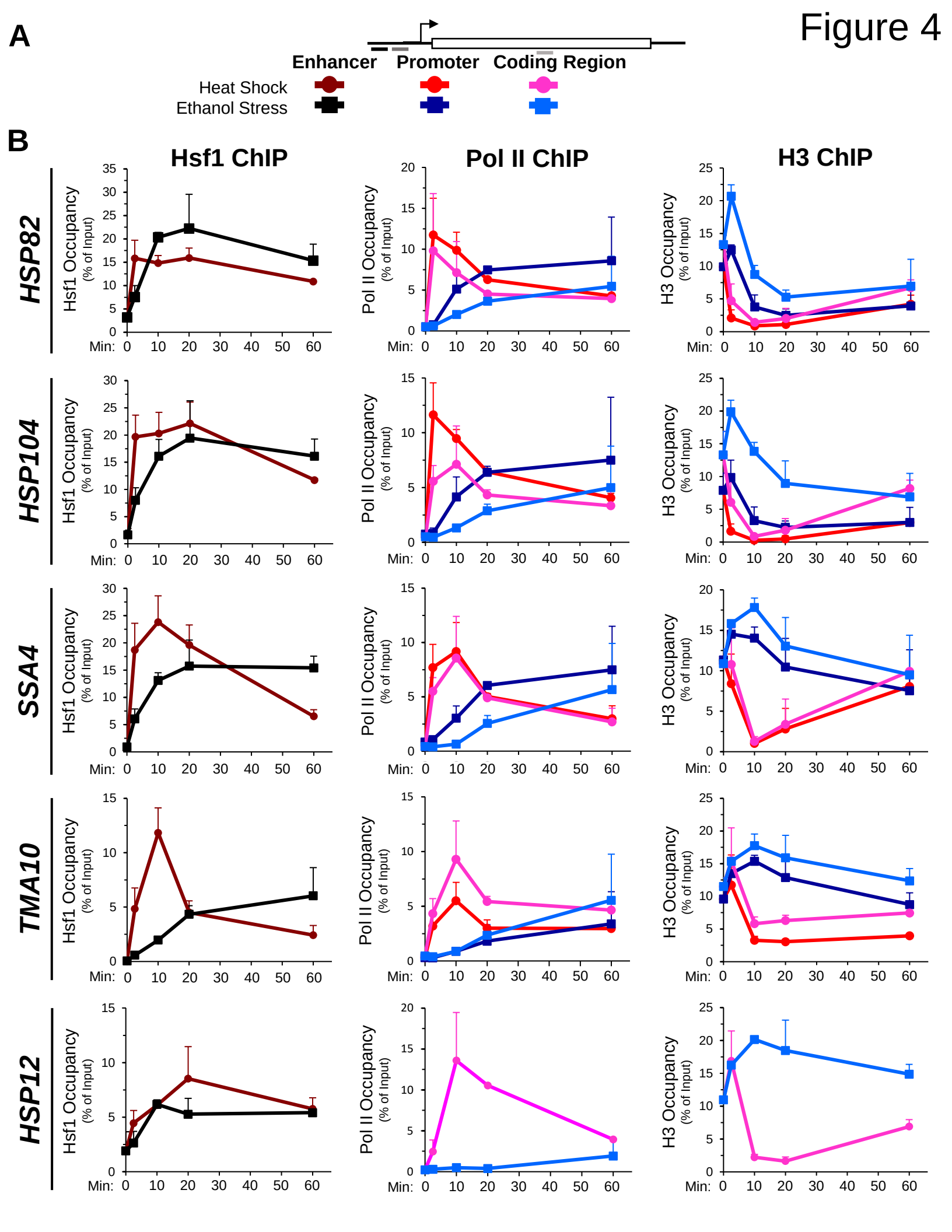
A
Enhancer
Promoter
Coding Region
Heat Shock
Ethanol Stress
B
Hsf1 ChIP
Pol II ChIP
H3 ChIP
HSP82
HSP104
SSA4
TMA10
HSP12
Hsf1 Occupancy (% of Input)
Pol II Occupancy (% of Input)
H3 Occupancy (% of Input)
Min: 0 10 20 30 40 50 60

Figure 4. Hsf1 and Pol II recruitment to *HSR* genes is delayed in ethanol stressed cells, while histone occupancy transiently increases.

(A) Map of a representative *HSR* gene depicting locations of primers used for chromatin immunoprecipitation (ChIP) analysis. Heat shock: shades of red and pink. Ethanol stress: shades of blue.

(B) ChIP analysis of Hsf1, Pol II (Rpb1) and histone H3 occupancy to the enhancer (UAS), promoter and coding regions of the indicated genes. Mid-log cultures of strain BY4741 were subjected to the indicated times of heat shock (39°C) or ethanol stress (8.5% v/v, 25°C). Time points evaluated for all three factors: 0, 2.5, 10, 20 and 60 min. Antibodies raised against full-length Hsf1, CTD of Rbp1 or the globular domain of Histone H3 were used (see **Materials and Methods**). ChIP signals were normalized to input. Shown are means + SD. N=2, qPCR=4.

Figure 5

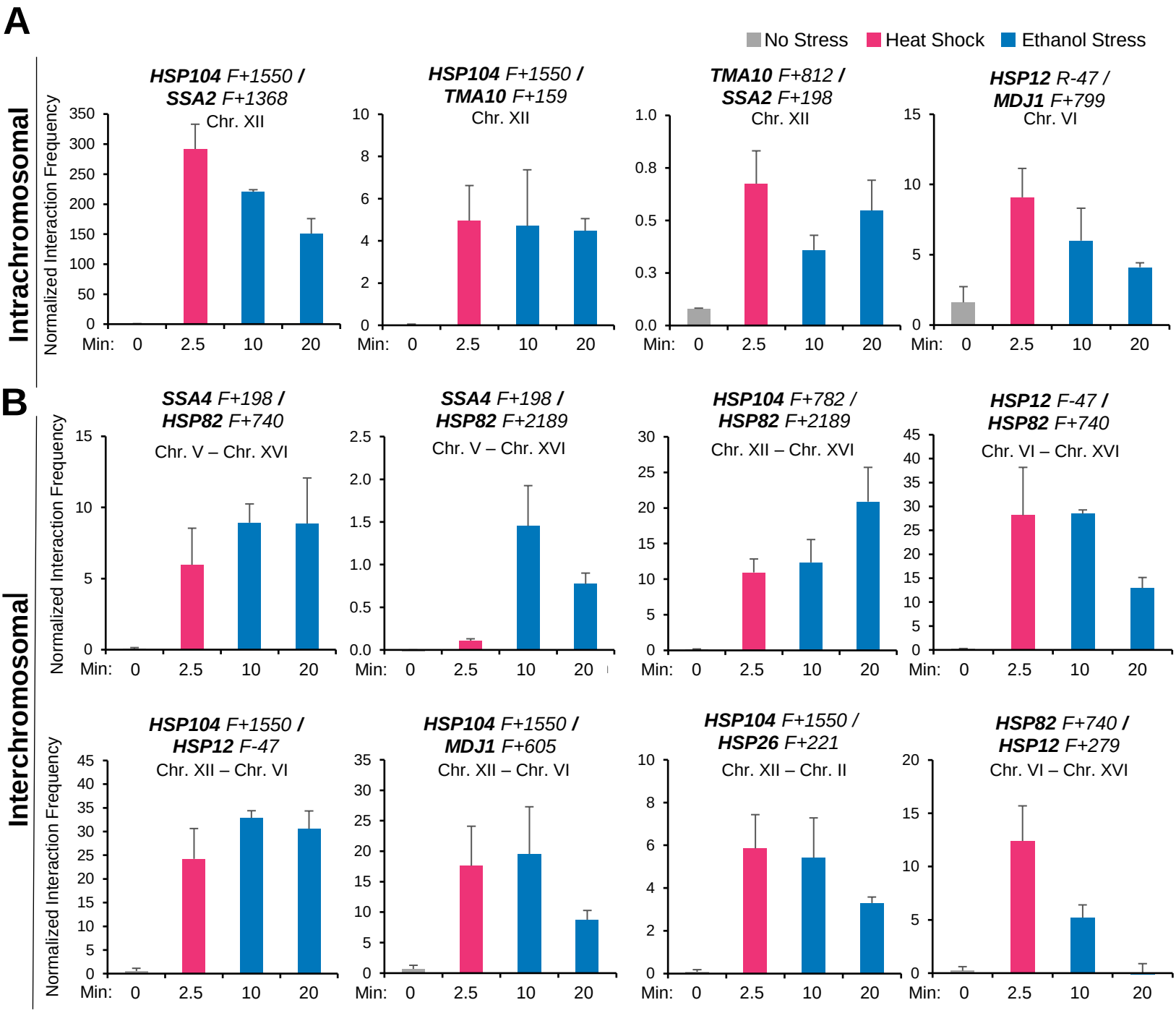

Figure 5. Ethanol stress induces intergenic interactions between *HSR* genes that are comparable to those induced by acute thermal stress.

(A) Intrachromosomal *(cis)* interactions between *HSR* genes were analyzed by Taq I-3C. W303-1B cells were instantaneously shifted from 30° to 39°C for 2.5 min (HS) or exposed to 8.5% v/v ethanol at 30°C for 10 or 20 min (ES). No stress samples were kept at 30°C. Location of Taq I coordinates are provided in **Figure 5–figure supplement 1**. F (forward) primers are positioned near the indicated Taq I restriction site. 3C signals were normalized to the 3C signal derived from using a naked genomic DNA template. Graphs depict means + SD; N=2; qPCR=4.

(B) Interchromosomal *(trans)* interactions between *HSR* genes were performed as in (A).

Figure 6

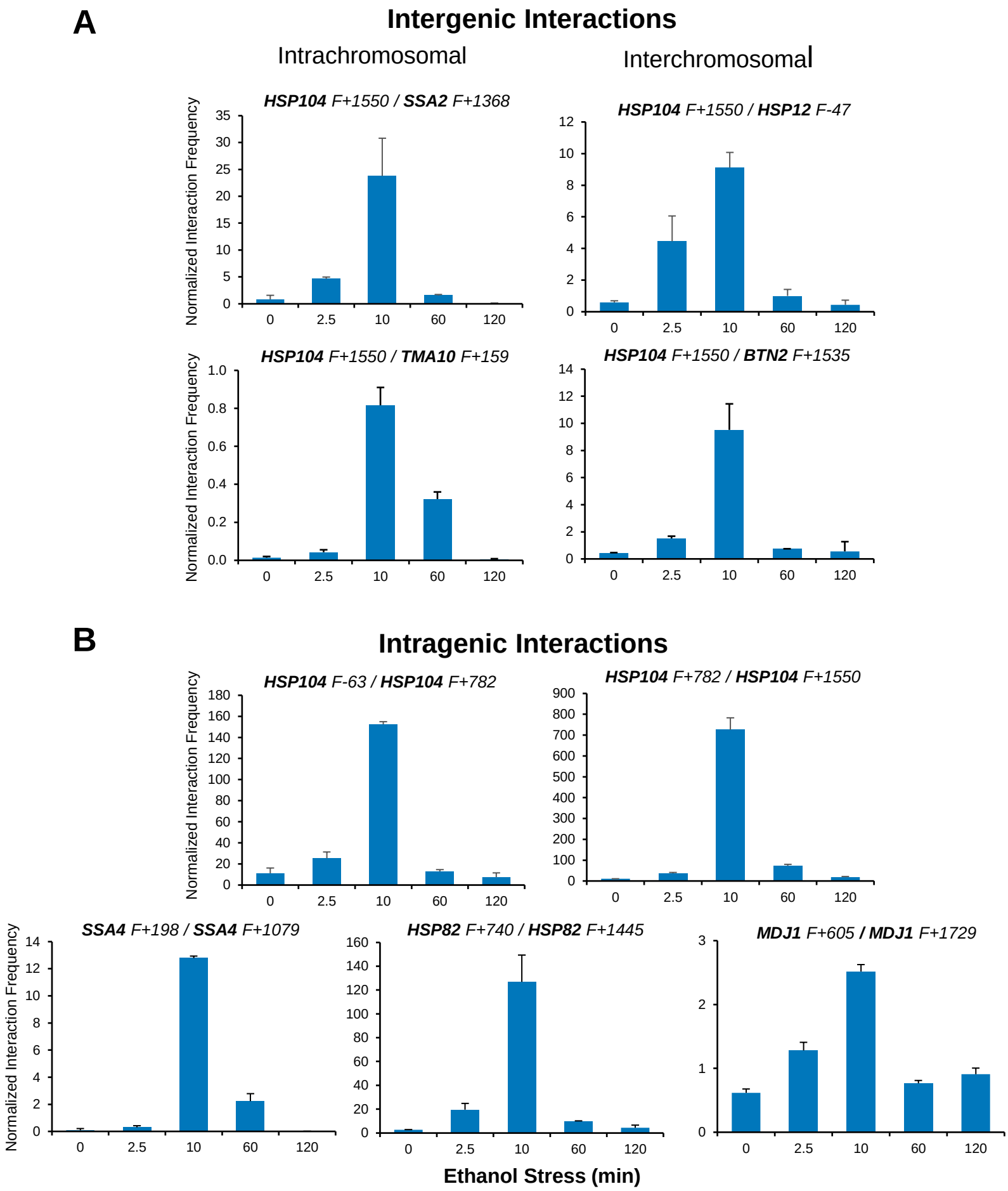
A
Intergenic Interactions
Intrachromosomal
Interchromosomal
HSP104 F+1550 / SSA2 F+1368
HSP104 F+1550 / HSP12 F-47
HSP104 F+1550 / TMA10 F+159
HSP104 F+1550 / BTN2 F+1535
Normalized Interaction Frequency
0
2.5
10
60
120
B
Intragenic Interactions
HSP104 F-63 / HSP104 F+782
HSP104 F+782 / HSP104 F+1550
SSA4 F+198 / SSA4 F+1079
HSP82 F+740 / HSP82 F+1445
MDJ1 F+605 / MDJ1 F+1729
Ethanol Stress (min)

Figure 6. Ethanol-induced *HSR* gene interactions are detectable by 2.5 min but typically dissipate within 60 min

(A) Taq I-3C analysis of intergenic interactions occurring during ethanol stress was conducted as described in **Figure 5**. All samples were kept at 25°C. Plotted are means + SD. N=2, qPCR=4.

(B) As in (A), but for intragenic interactions.

Figure 7

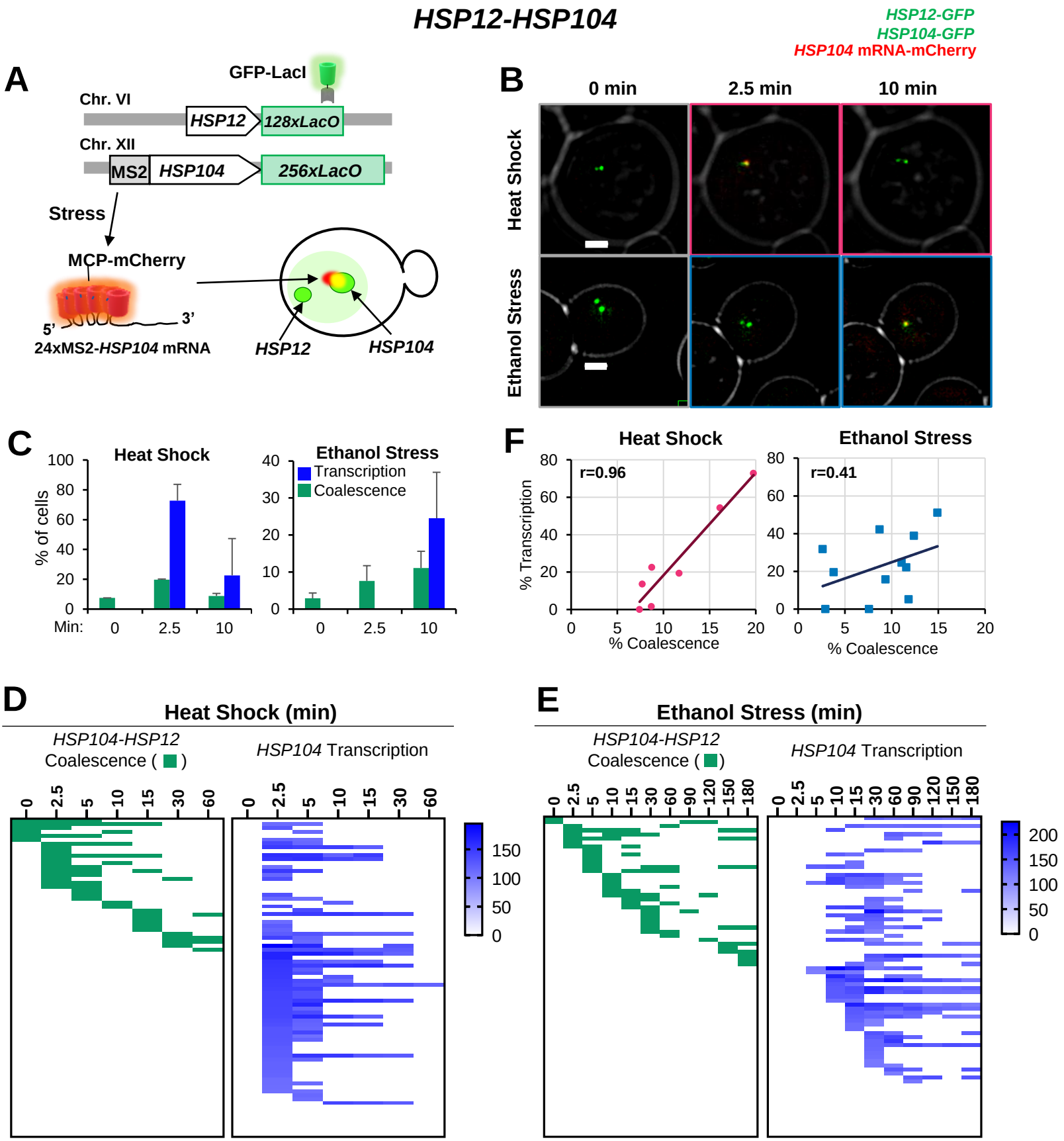
HSP12-HSP104
A
GFP-LacI
Chr. VI
HSP12
128xLacO
Chr. XII
MS2
HSP104
256xLacO
Stress
MCP-mCherry
5'
3'
24xMS2-HSP104 mRNA
HSP12
HSP104
B
HSP12-GFP
HSP104-GFP
HSP104 mRNA-mCherry
0 min
2.5 min
10 min
Heat Shock
Ethanol Stress
C
Heat Shock
Ethanol Stress
Transcription
Coalescence
% of cells
Min:
F
r=0.96
r=0.41
% Transcription
% Coalescence
D
Heat Shock (min)
HSP104-HSP12
Coalescence
HSP104 Transcription
E
Ethanol Stress (min)

Figure 7. *HSR* gene transcription and coalescence are strongly correlated in heat-shocked but not ethanol-stressed cells.

(A) *HSP12* and *HSP104* are flanked by *LacO* arrays in the heterozygous diploid strain VPY705. In addition, *HSP104* has a 24xMS2 loop array integrated within its 5'-UTR. MCP-mCherry binds to the nascent chimeric *HSP104* transcript and is visualized as a red dot adjacent to the gene which appears as a green dot.

(B) Live cell confocal fluorescence microscopy of strain VPY705 heat-shocked at 39°C using a VAHEAT device or exposed to 8.5% ethanol at 25°C for the indicated times. An Olympus spinning disk confocal microscope system was used for imaging. Scale bar: 2 µm.

(C) Quantification of VPY705 cells treated as above and scored for the coalescence of *HSP104-HSP12* and the presence of chimeric *MS2x24-HSP104* mRNA. Cells were scored positive for coalescence only when a single green dot could be visualized in the nucleus across the 11 z-planes. Transcription was scored as positive only when a red dot above background could be seen near the large green dot (*HSP104*). Approximately 40 cells were scored per timepoint, per condition. Graphs represent means + SD. N=2.

(D) Single cell analysis of *HSP12-HSP104* coalescence (green) and *HSP104* transcription (blue) at discrete timepoints over a heat shock time course. Each row in the transcription analysis corresponds to the same cell in the coalescence analysis. Blue gradient represents the intensity of mCherry signal in each cell.

(E) As in (D) but for ethanol stress.

(F) Scatter plot showing the correlation (r) between percent transcription and percent coalescence in HS and ES cells (derived from D and E). Each plotted value corresponds to a different stress timepoint (see also **Figure 7 – figure supplement 1D**).

Figure 8

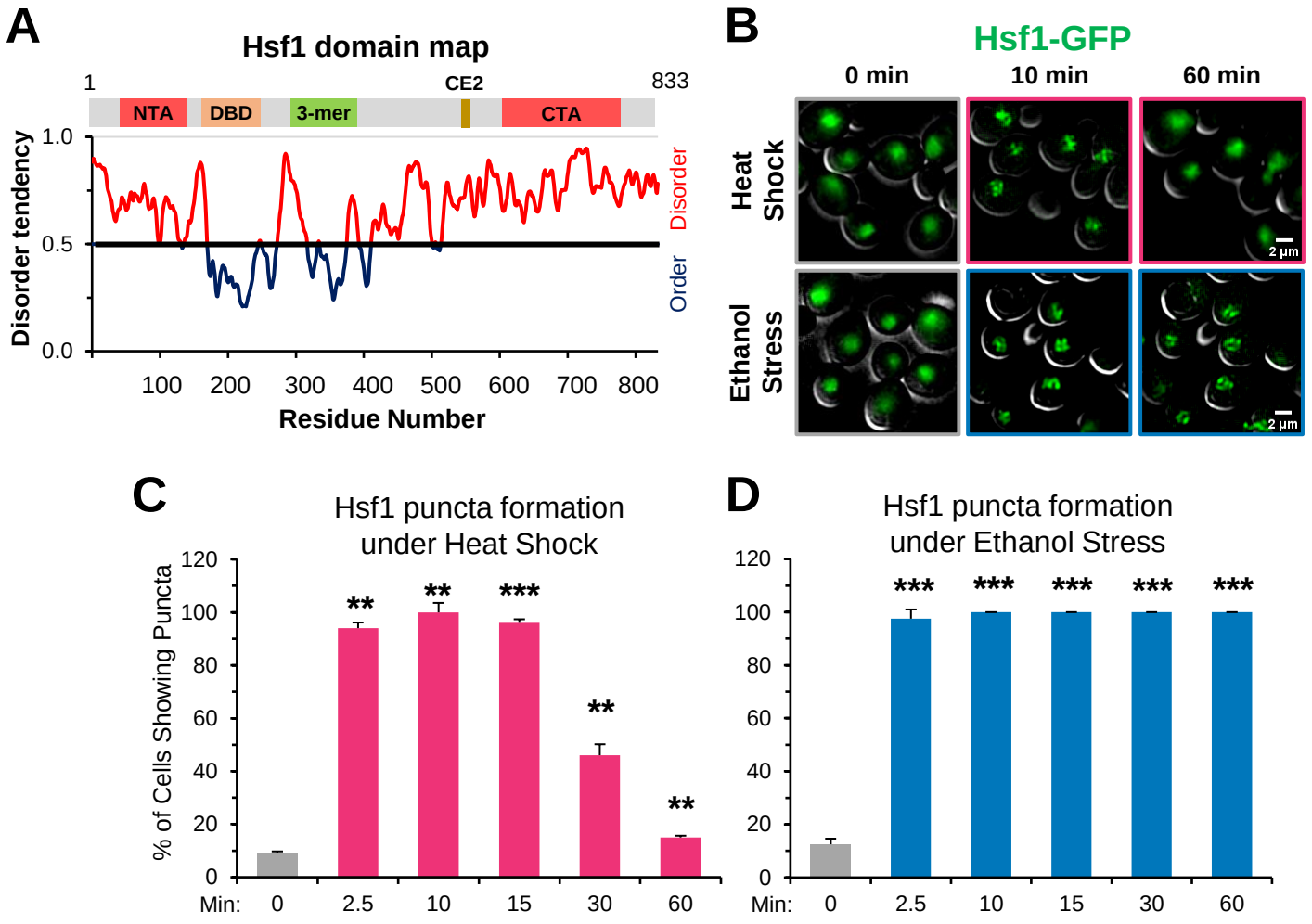

Figure 8. Ethanol stress induces rapid formation of long-lasting Hsf1 condensates

(A) Hsf1 is a transcription factor bearing N- and C-terminal domains with high disorder tendency (determined by IUPRED2). NTA, N-terminal activator; DBD, DNA binding domain; 3-mer, trimerization domain; CE2, conserved element 2 (Hsp70 binding site); CTA, C-terminal activator.

(B) Hsf1-GFP condensates form in response to ethanol stress. Diploid cells expressing Hsf1-GFP (ASK741) were grown in synthetic complete medium supplemented with adenine (SDC + Ade) and mounted onto ConA-coated coverslips. Live cell widefield microscopy was performed on cells exposed to either heat shock (38°C) or ethanol stress (8.5% v/v) or left untreated (25°C). A representative plane is shown for each condition out of 11 z-planes imaged (interplanar distance of 0.5 µm). Scale bar: 2 µm.

(C) ASK741 cells were subjected to a 38°C heat shock for the indicated times and scored for the presence of Hsf1 condensates. A cell was scored as positive if it contained at least one clearly defined puncta. Approximately 200 cells were evaluated per timepoint. A one-tailed t-test was used to assess significance (stress versus no stress condition). N=2. **, *p<0.01;* ***, *p<0.001.*

(D) ASK741 cells were exposed to 8.5% v/v ethanol for the indicated times and the presence of Hsf1 condensates were scored from a total of 200 cells per timepoint. Significance was determined as in (C).

Figure 9

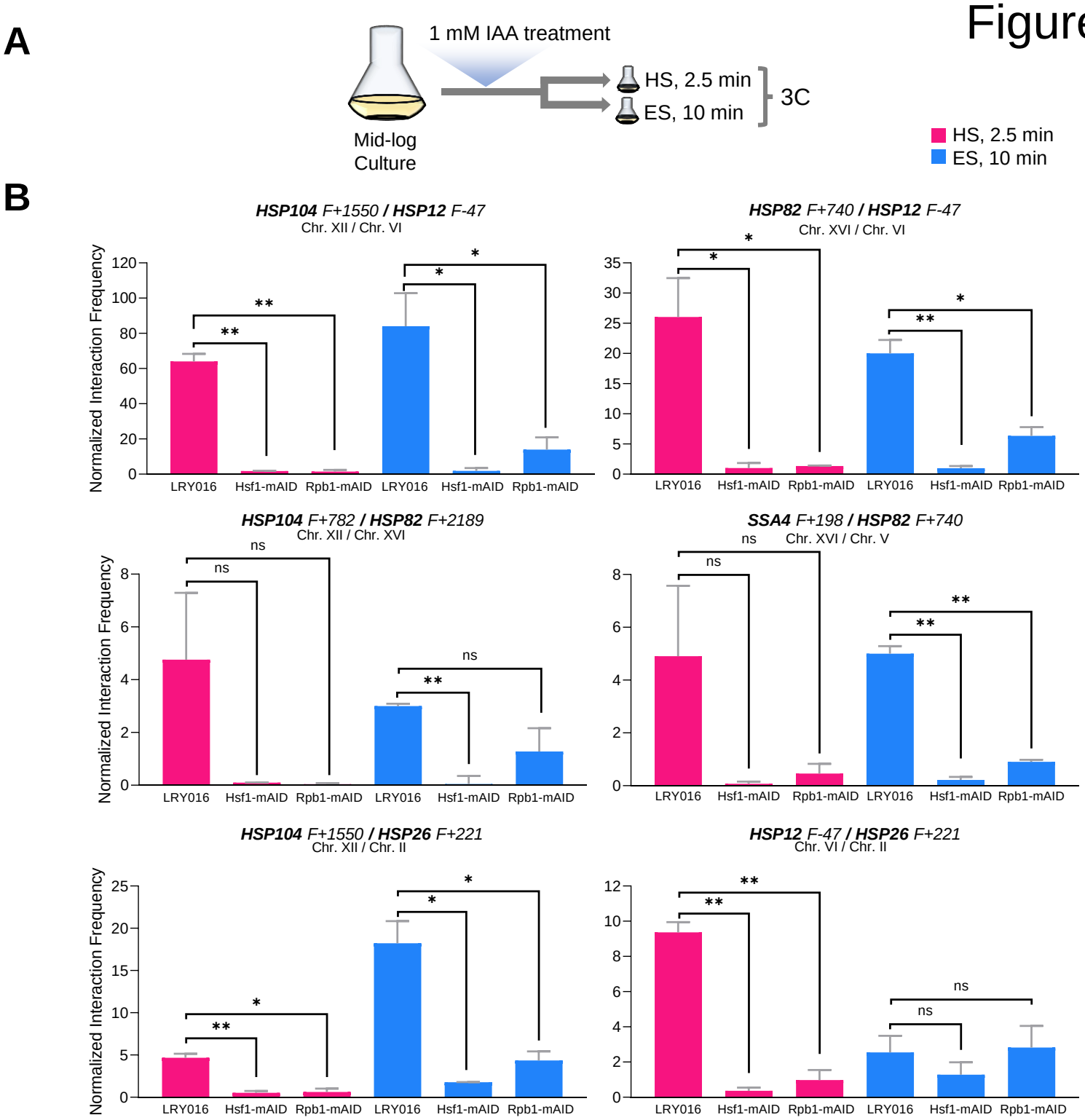

Figure 9. Hsf1 and Pol II are critically required for *HSR* gene interactions in response to either heat shock or ethanol stress

(A) Experimental strategy. Degron-tagged cells were treated with 1 mM IAA at 25°C for 30-40 min prior to exposure to either heat shock (HS, 39°C for 2.5 min) or ethanol stress (ES, 8.5% v/v ethanol for 10 min) followed by HCHO crosslinking and 3C analysis.

(B) Strains LRY016 (W303-1B; OsTIR1), LRY100 (LRY016; Hsf1-mAID) and LRY102 (LRY016; Rpb1-mAID) were subjected to the above protocol and physical interactions between the indicated chromosomal loci were detected by Taq I-3C as in **Figure 5**. Representative interchromosomal interactions are shown. Graphs represent means + SD. Statistical significance between the indicated interaction frequencies was determined using a one-tailed t-test. *, $p<0.05$; **, $p<0.01$; ns, not significant. A no stress sample, maintained at 30°C for 10 min following IAA treatment and then crosslinked, was handled in parallel. No signal above background was detected for any pairwise test.

Figure 10

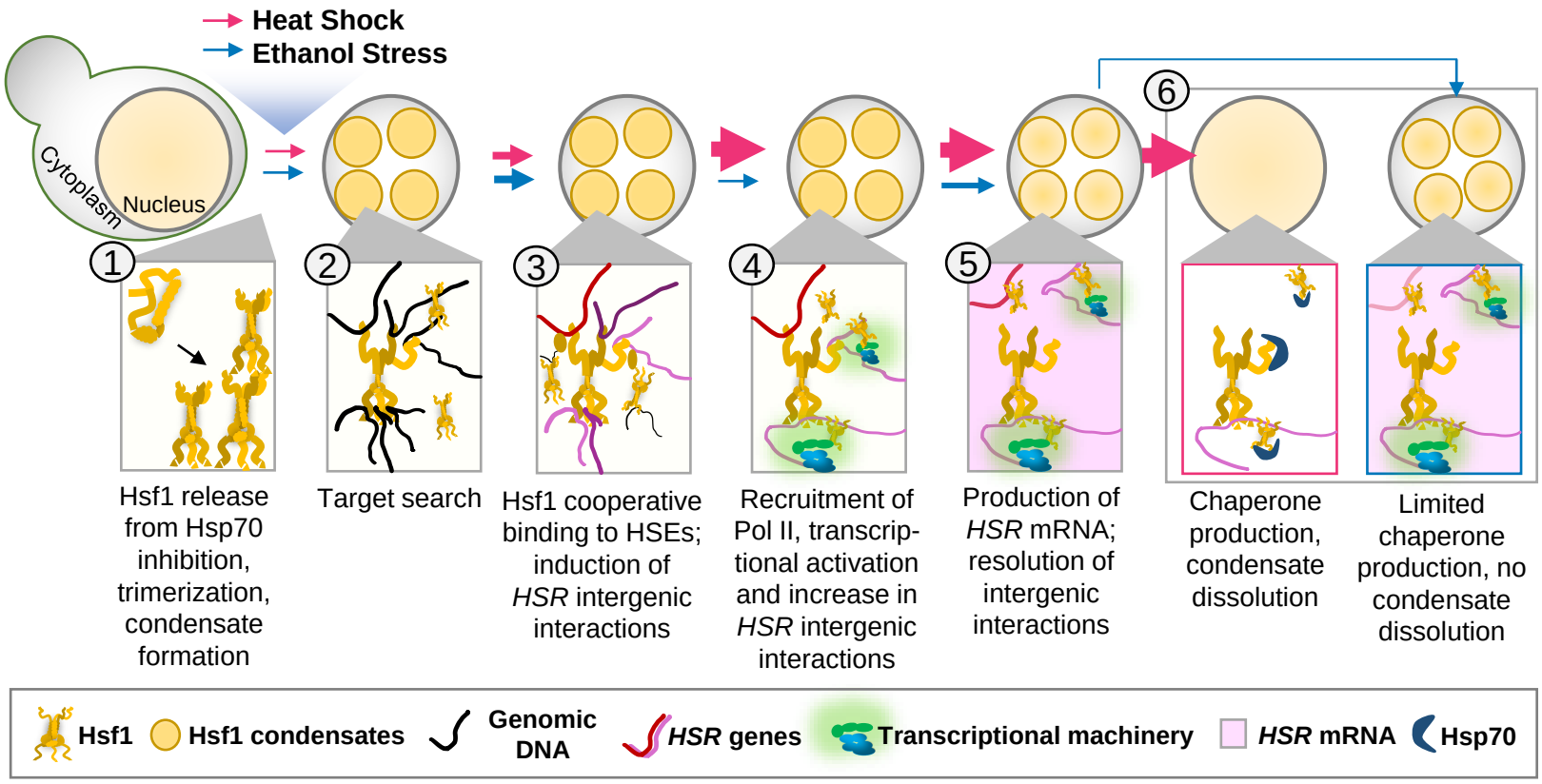

Figure 10. Hsf1 forms condensates, restructures the genome and transcriptionally activates *HSR* genes in response to both thermal and chemical stresses but does so with strikingly different kinetics.

Heat Shock (pink arrows): *S. cerevisiae* cells exposed to heat shock (30° to 39°C upshift) undergo protein misfolding (proteotoxicity), leading to chaperone titration and activation of Hsf1 accompanied by formation of Hsf1 condensates (**1).** Rapid target search is hypothesized to occur via multivalent interactions between Hsf1's activation domains and chromatin-bound proteins (Brodsky et al., 2020) (**2**). Subsequently, Hsf1 cooperatively binds HSEs and induces the 3D reorganization of *Heat Shock Responsive (HSR*) genes (**3**). Simultaneously, RNA Pol II is recruited to *HSR* genes and transcription is induced (**4**). Productive transcription (pink shading) ensues, followed by dissolution of *HSR* gene interactions (**5**). Rapid export of *HSR* mRNAs (Zander et al, 2016) facilitates production of chaperone and cytoprotective proteins, which aid in restoration of proteostasis and disassembly of Hsf1 condensates (Chowdhary et al, 2022) (**6**).Thickness of arrows (for both HS and ES) symbolizes rapidity and/or magnitude of the subsequent step.

Ethanol Stress (blue arrows): Exposure to 8.5% (v/v) ethanol induces proteotoxicity, titration of chaperones, and subsequent activation of Hsf1, triggering formation of condensates (**1, 2**). Condensates may aid Hsf1 target search by facilitating the multivalent interactions described above (**2**). Hsf1 then binds HSEs, inducing *HSR* gene repositioning (**3**). Subsequently, Pol II is recruited and transcriptionally activated (**4**). Ethanol stress-induced interactions dissipate well before maximal *HSR* gene transcriptional induction is achieved (**5**). The weak transcriptional *HSR* gene output, coupled with suppressed *HSR* mRNA export under ES (Izawa et al, 2008), results in a low level of chaperone synthesis (**6**) that fails to resolve proteotoxicity. This likely contributes to the persistence of Hsf1 condensates.

Figure 11

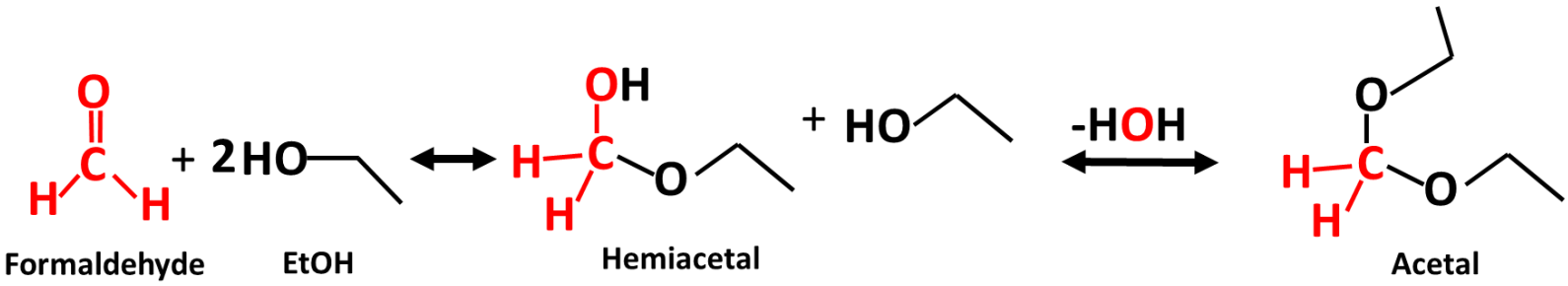

Figure 11. Acetal formation reaction (McMurry, 2012)

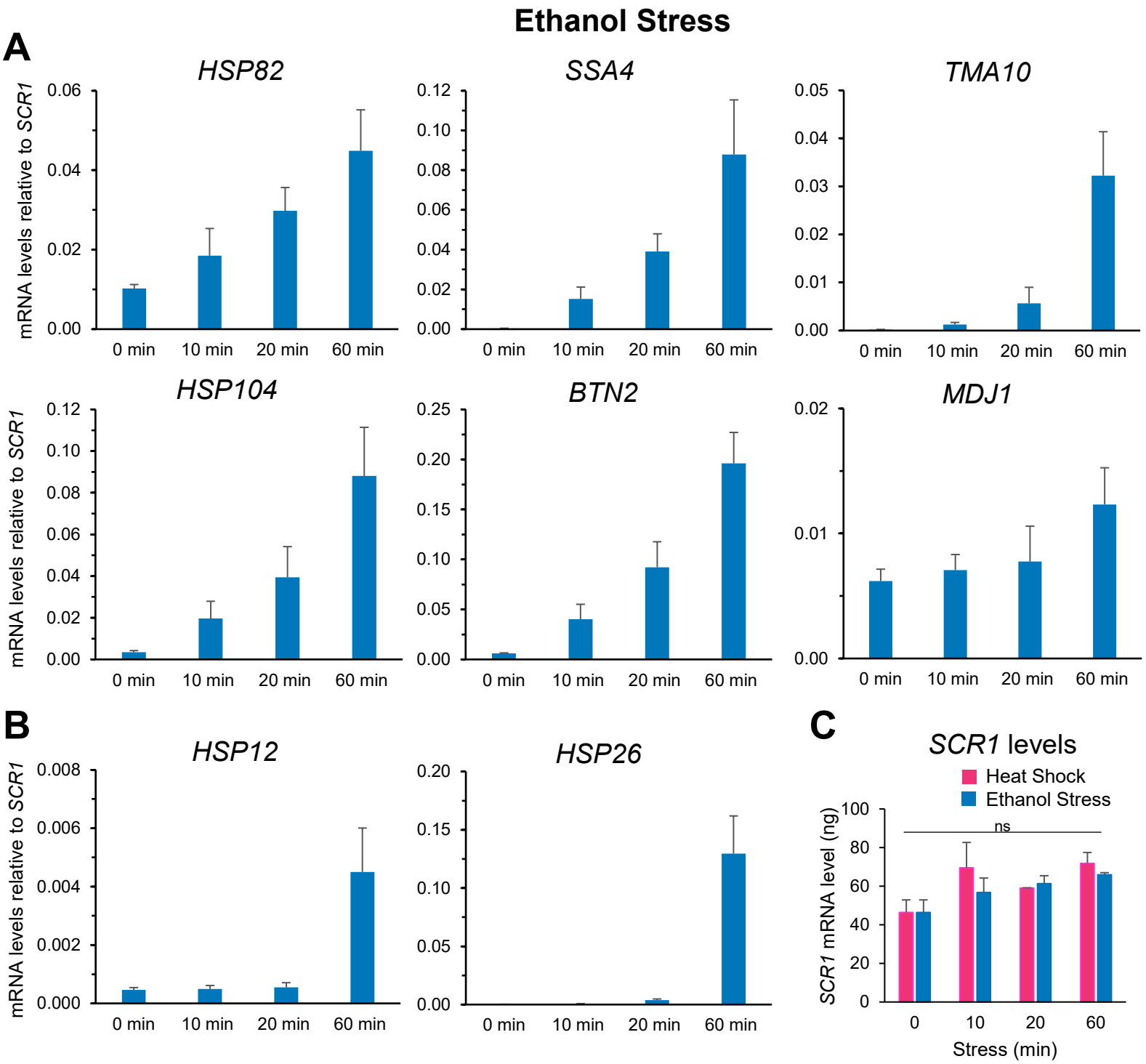

Figure 3 – figure supplement 1. Ethanol stress transcriptionally induces *HSR* genes.

(A) RNA abundance of Hsf1-dependent genes was determined as in Figure 3. Cells were exposed to 8.5% (v/v) ethanol at 25°C for the indicated times. Depicted are means + SD. N=2, qPCR=4.

(B) As in (A), but the Hsf1-, Msn2-dual regulated genes *HSP12* and *HSP26* were evaluated.

(C) Quantification of *SCR1* mRNA levels used for normalization of transcripts, analyzed by RT-qPCR. N=2, qPCR=4. A one-way ANOVA test (GraphPad Prism 8.0) was performed. ns (not significant), P>0.05.

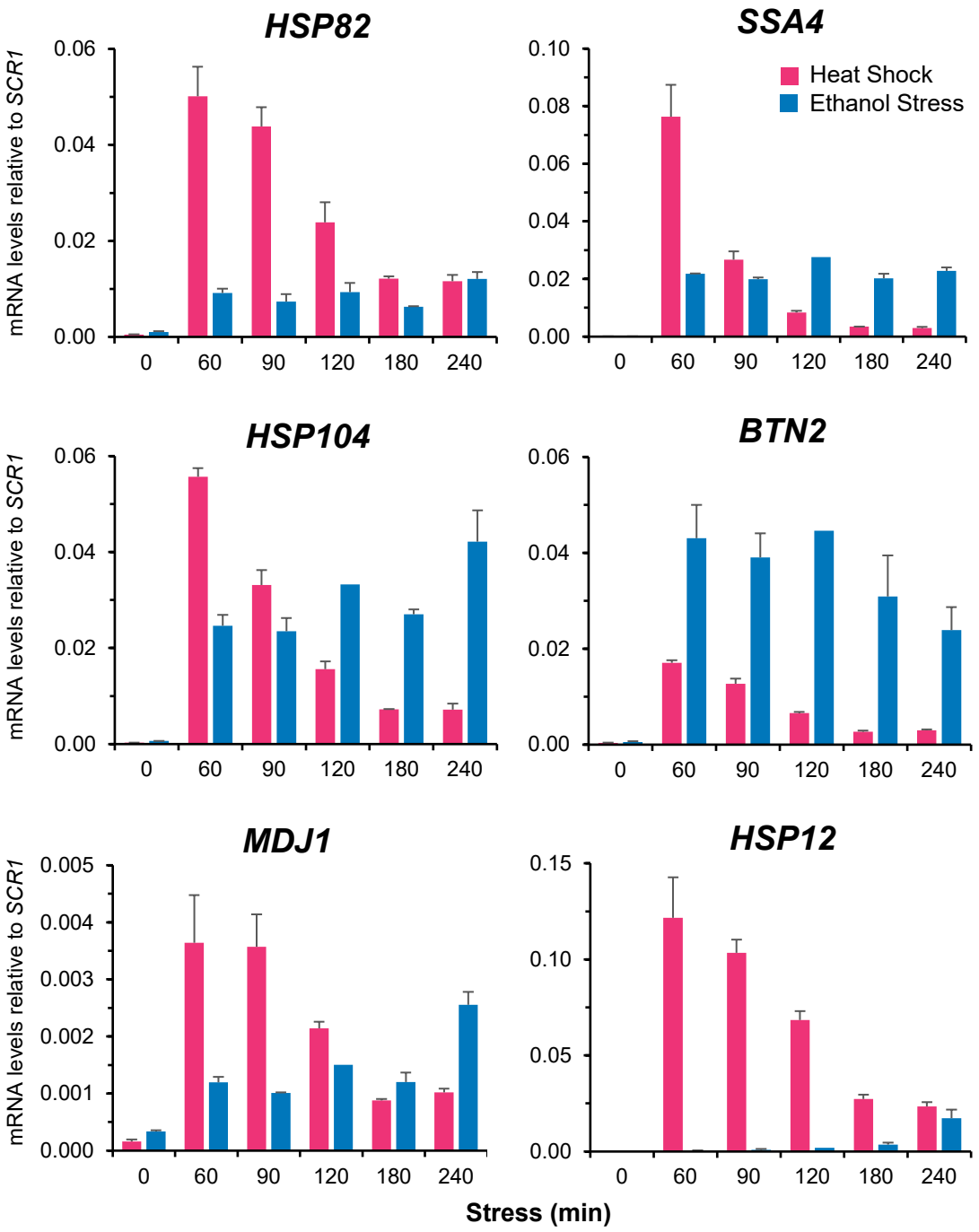

Figure 3 – figure supplement 2. In response to chronic heat stress *HSR* mRNA levels gradually attenuate, whereas in response to chronic ethanol stress they remain constant.

Abundance of *HSR* mRNAs was determined by RT-qPCR. Experiment was conducted as described in Figure 3 except longer time points were evaluated. Depicted are means + SD. N=2, qPCR=4.

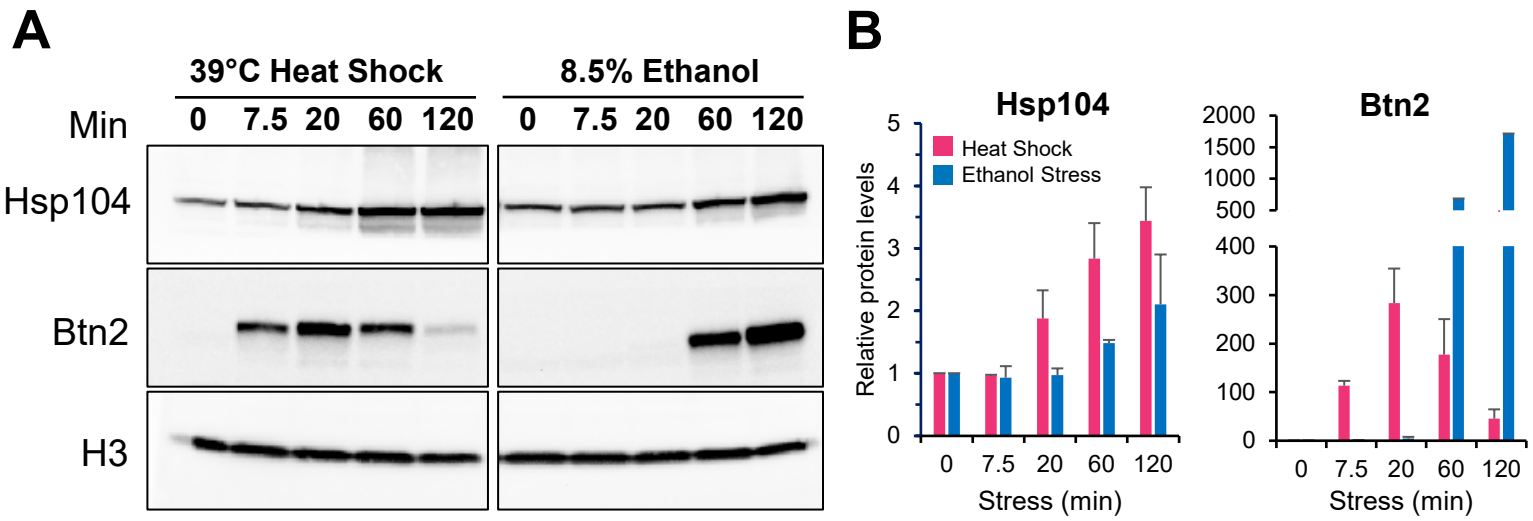

Figure 3 – figure supplement 3. Induced HSR protein production is evident early during heat shock while it is delayed during ethanol stress.

(A) Analysis of chaperone levels by Immunoblot. Strain W303-1B was exposed to constant heat shock or ethanol stress conditions for different timepoints. Levels of Histone H3, Hsp104, and Btn2 were monitored using antibodies against endogenous proteins. Histone H3 serves as the loading control.

(B) Quantification of Hsp104 and Btn2 protein levels, samples were treated as described in (A). Protein levels were normalized to histone H3 and 0 min timepoints. Shown are means + SD. N=2.

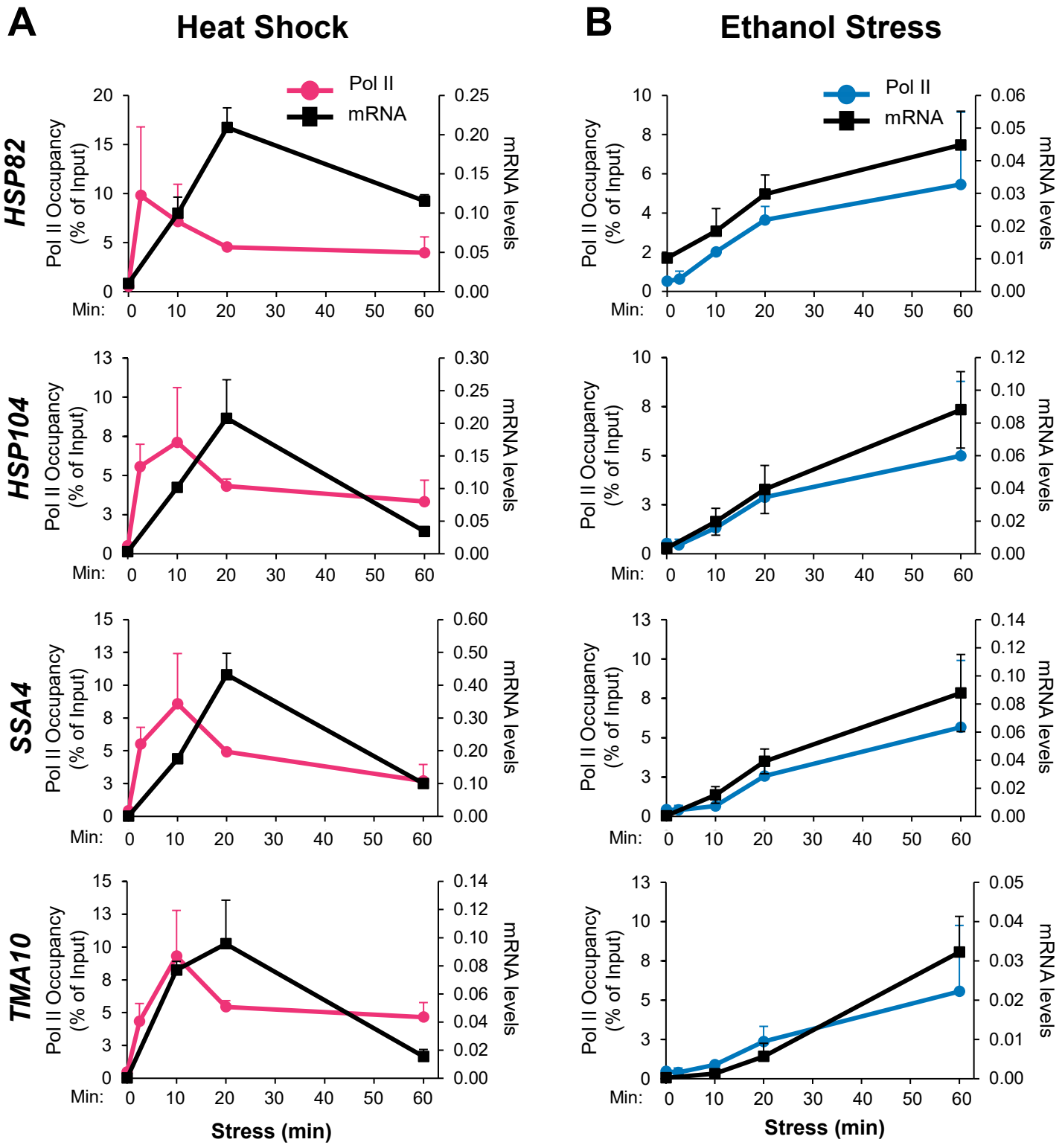

Figure 4 – figure supplement 1. Pol II occupancy of the indicated *HSR* genes vs. their mRNA levels in cells subjected to either heat shock or ethanol stress.

(A) Pol II ChIP and RT-qPCR data of the indicated *HSR* genes in cells exposed to HS are co-plotted to allow comparison of the occupancy of Pol II (over ORF) versus the corresponding transcript levels. Data derived from Figures 2A and 3.

(B) As above, except for ethanol stress.

Figure 4 – figure supplement 2

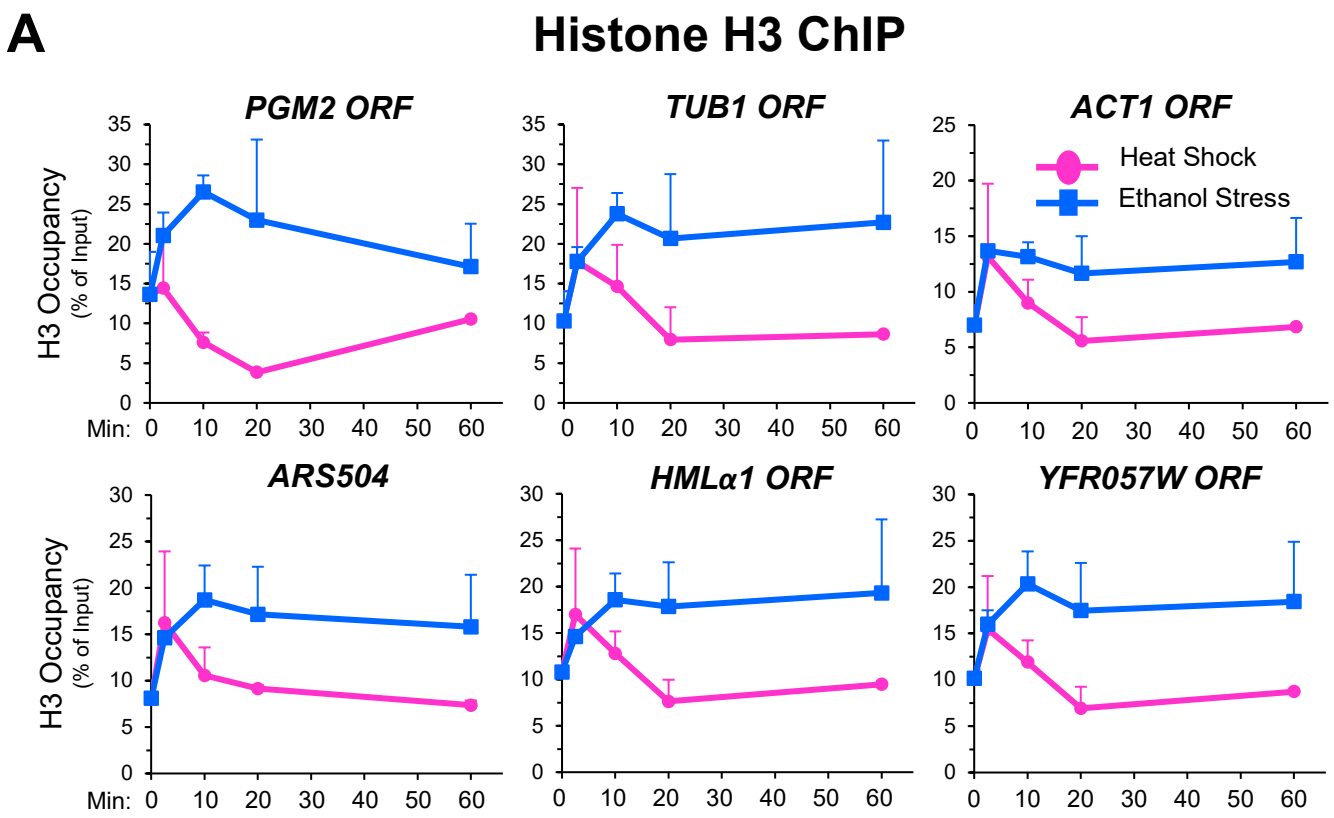

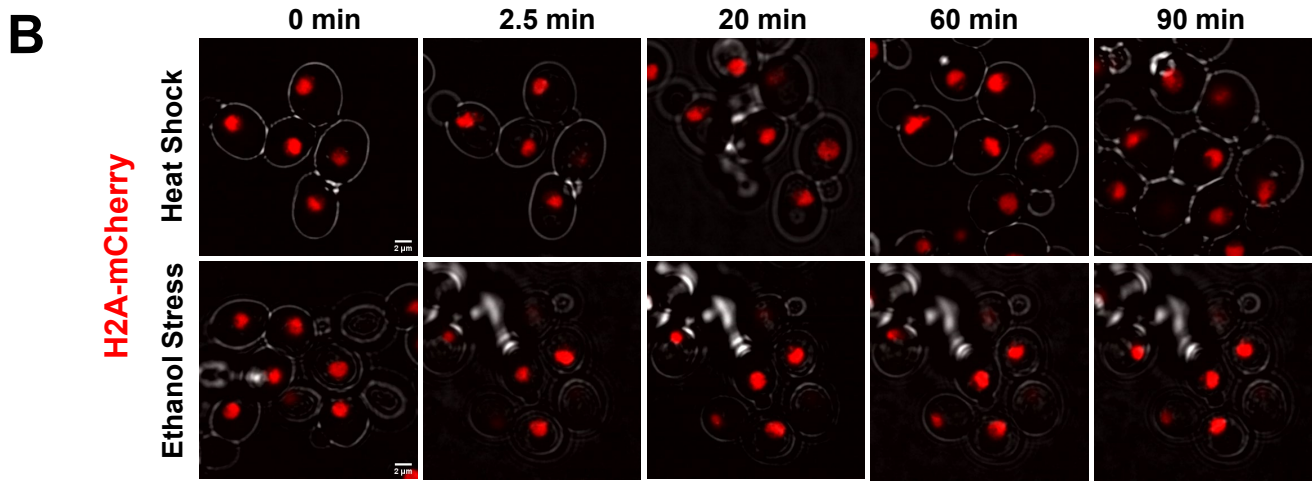

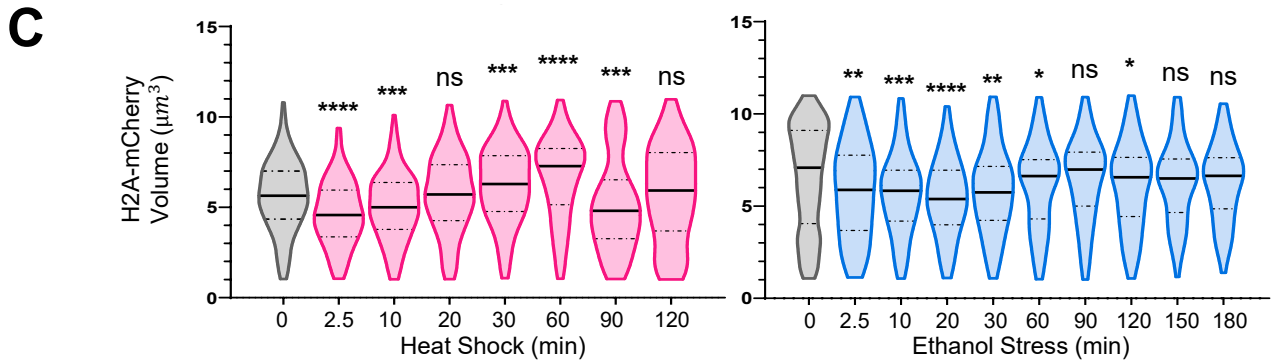

Figure 4 – figure supplement 2. Ethanol and thermal stresses induce chromatin compaction.

(A) ChIP analysis of histone H3 occupancy at inducible (*PGM2*), constitutive (*ACT1*, *TUB1*), and inactive/silenced loci (*ARS504, HMLα1, YFR057W*). Experiment was carried out and data quantified as in Figure 3B. Shown are means + SD. N=2, qPCR=4.

(B) Live cell confocal fluorescence microscopy of the diploid strain DBY1447. Histone H2A-mCherry was used to measure chromatin volume in cells cultivated in SDC medium at 25°C and then subjected to thermal (39°C) or ethanol stress (8.5% v/v) for the times indicated. VAHEAT device was used for heat shock (see Materials & Methods). Imaging was done across 11 z-planes with 0.5 µm of interplanar distance. Representative single plane images are shown. Scale bar: 2 µm.

(C) Violin plots depicting H2A-mCherry volume measurements of DBY1447 cells treated as in (B). An average of 100 cells per timepoint, per condition, were evaluated. H2A-mCherry volume was determined using 3D Objects Counter in ImageJ/Fiji (v. 1.54f). Statistical significance between no stress (0 min) and stress (2.5 – 180 min) samples was determined using Mann Whitney U Test. N=2. *, $p<0.05$; **, $p<0.01$; ***, $p<0.001$; ****, $p<0.0001$; *ns,* not significant.

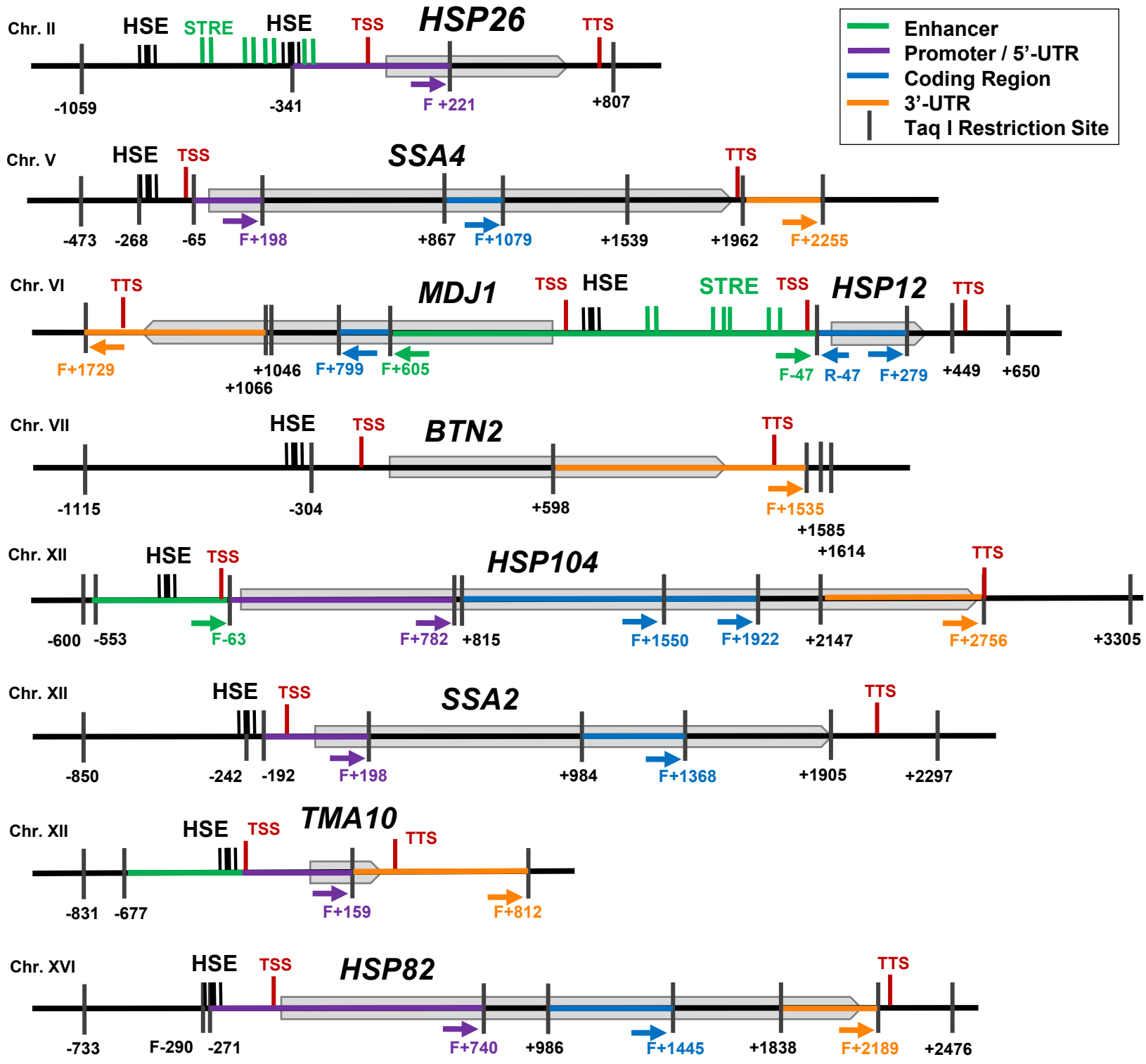

Figure 5–figure supplement 1. Physical maps of genes used in this study.

Taq I restriction sites are numbered relative to the ATG (+1) codon. Coding regions are represented by grey boxes. Locations of Hsf1 binding sites (Heat Shock Elements (HSEs)) are shown as triple black vertical lines. Stress Responsive Elements (STREs) (Msn2 binding sites) are shown as green vertical lines (shown only for select genes). The primers used to analyze 3C interactions are represented as arrows. TSS, Transcription Start Site. TTS, Transcription Termination Site.

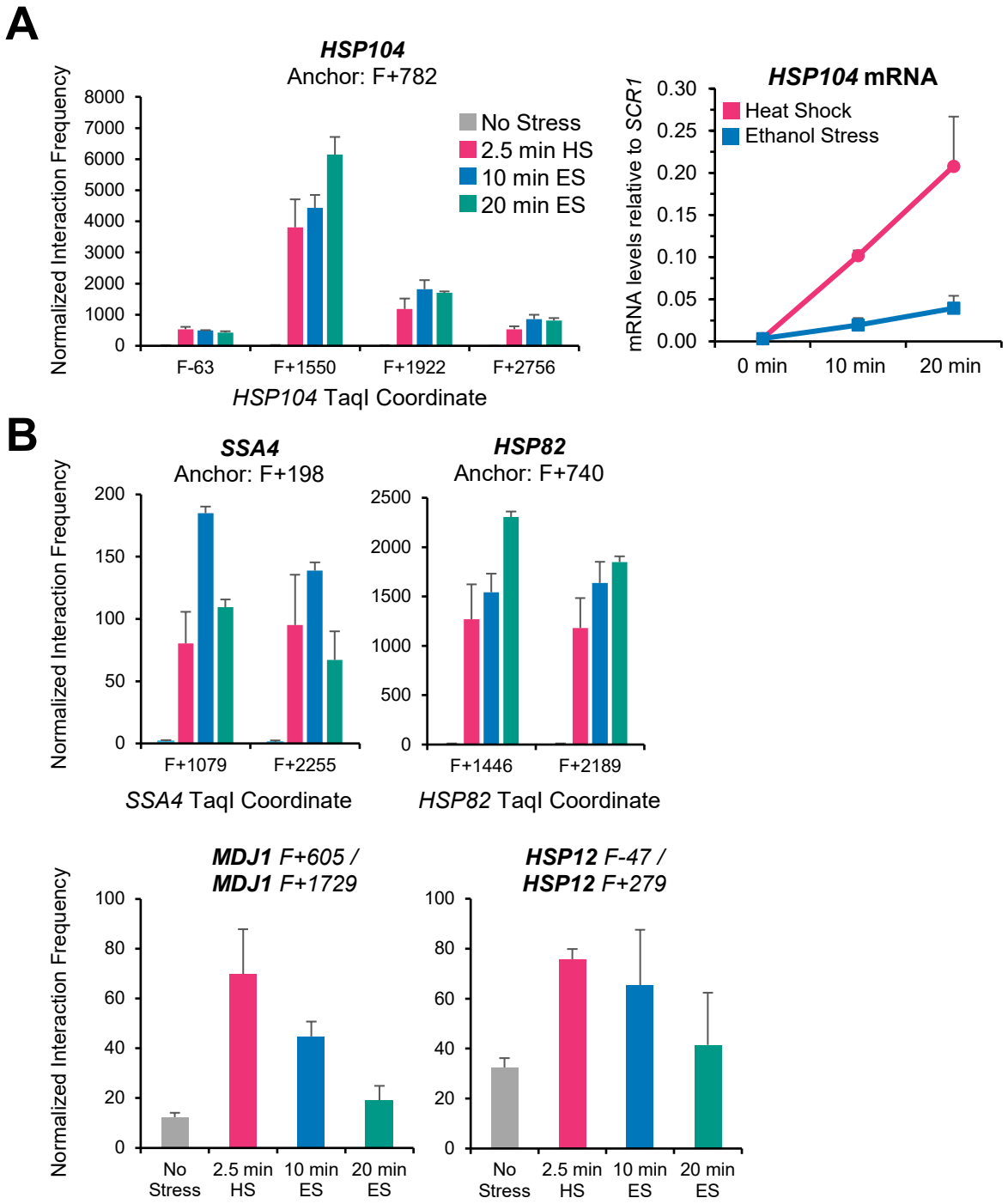

Figure 5–figure supplement 2. Intragenic interaction frequency induced by ethanol stress is comparable to those induced by thermal stress, despite modest transcriptional output.

(A) Comparison of *HSP104* intragenic interactions (left) with *HSP104* mRNA levels (right). Samples from strain W303-1B were exposed to thermal (HS, 39°C) or ethanol stress (ES, 8.5%) for the indicated times. Intragenic interactions were analyzed by Taq I-3C; mRNA data are from **Figure 3A**. Locations of Taq I restriction sites are in **Figure 5–figure supplement 1**. Depicted are means + SD. N=2, qPCR=4.

(B) Taq I-3C analysis of intragenic interactions of the indicated Hsf1 target genes. Analysis and symbols as in (A).

Figure 7–figure supplement 1

TMA10-HSP104

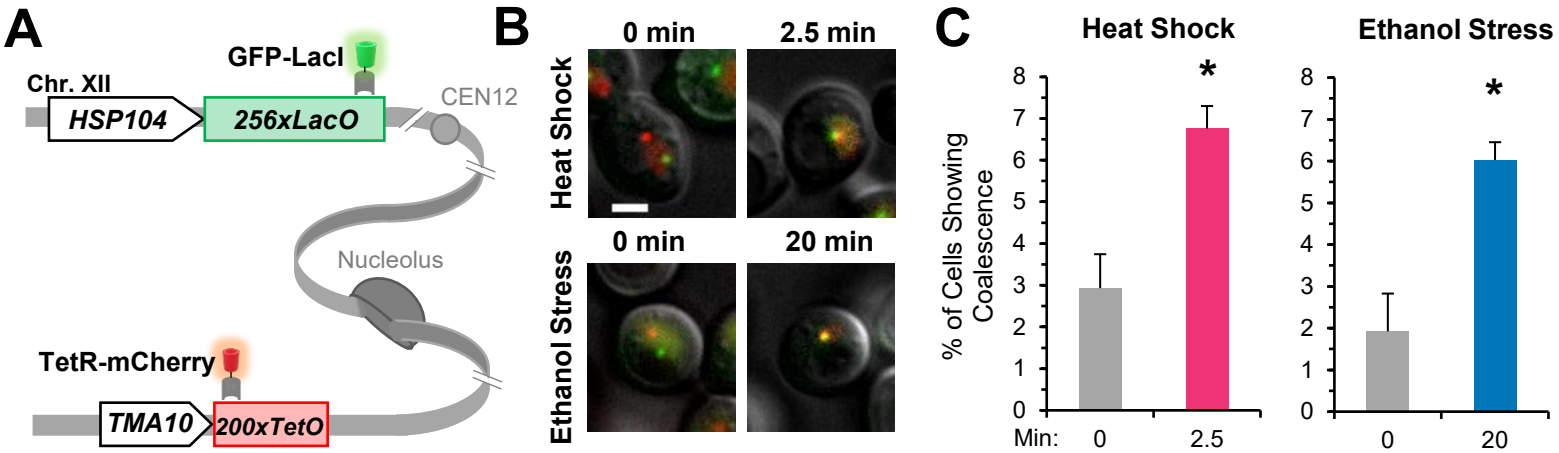

HSP12-HSP104

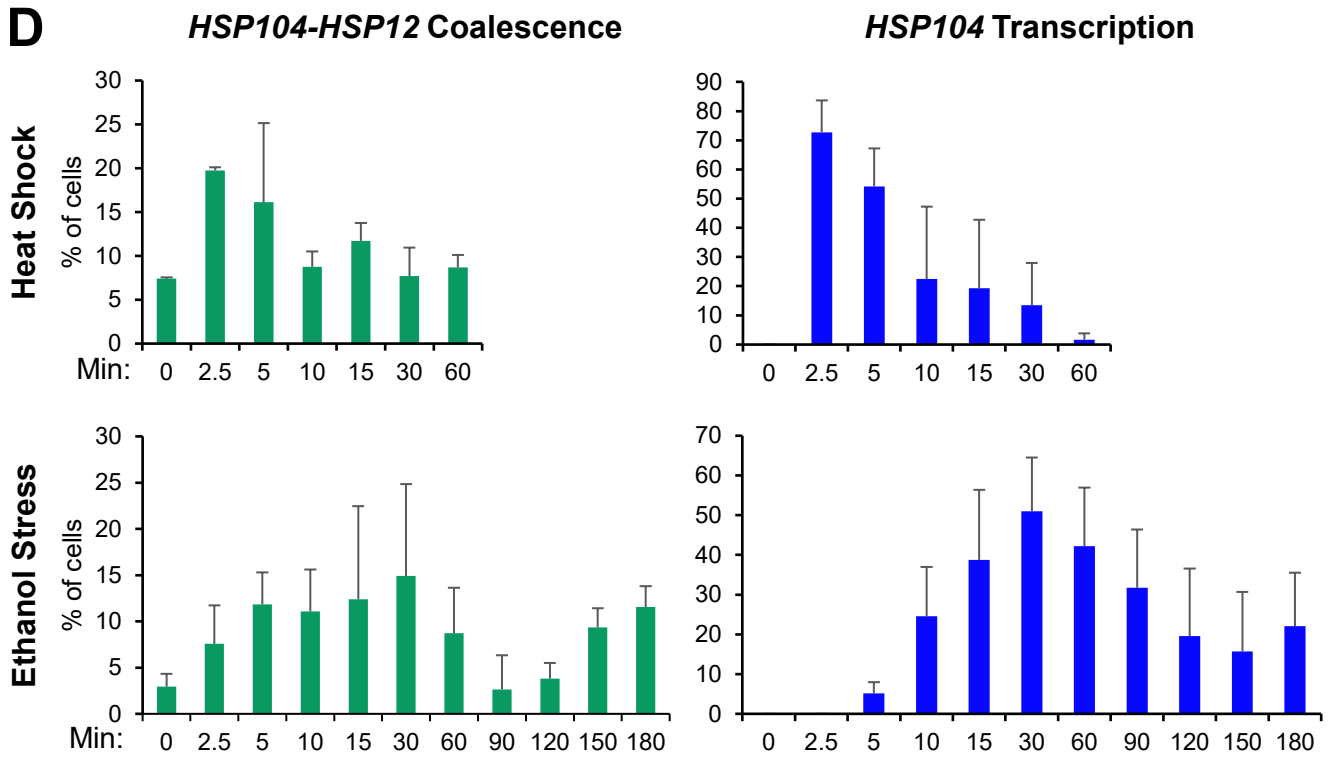

Figure 7–figure supplement 1. *HSR* gene coalescence and transcription are temporally uncoupled in ethanol stressed cells.

(A) Relative location of *HSP104* and *TMA10* on Chr. XII in the diploid strain ASK727. One allele of *HSP104* is flanked by an integrated $LacO_{256}$ array and one allele of *TMA10* is flanked by a $TetO_{200}$ array. ASK727 also expresses GFP-LacI and TetR-mCherry (N- and C-terminal fusion, respectively) to allow visualization of the two genes as a green and red dot, respectively.

(B) Live cell widefield fluorescence microscopy of ASK727. Cells were immobilized onto ConA-coated coverslips and exposed to either heat shock (25°C to 38°C upshift) or ethanol stress (8.5% v/v; 25°C) for the indicated times (see Materials & Methods). 11 z-planes with 0.5 µm interplanar distance were captured for each condition. A representative z-plane is shown per condition. Scale bar: 2 µm.

(C) ASK727 cells, treated as in B, were scored for colocalization of *HSP104* and *TMA10* upon exposure to either heat shock or ethanol stress. A cell was scored as positive when the highest intensity signal from both genes overlapped in the same z-plane. An average of 70 cells were evaluated per condition, per timepoint. Displayed are means + SD. N=2. A one-tailed t-test was performed to assess significance. **, p<0.01. Note:* we interpret *HSP104-TMA10* coalescence observed at T=0 min to principally reflect coincidental overlap given absence of 3C signal under the no stress condition. A similar consideration applies to the *HSP104-HSP12* gene pair analyzed below.

(D) VPY705 cells were subjected to heat shock (39°C; VAHEAT device) or ethanol stress (8.5%) for the indicated times and imaged using an Olympus Spinning Disk Microscope System. Imaging was acquired over 11 z-planes, with 0.5 µm of distance between planes. *Left:* Percentage of cells showing coalescence between GFP-labeled alleles of *HSP104* and *HSP12*. *Right:* Percentage of cells in the population displaying an mCherry dot (MCP-mCherry bound *HSP104* transcripts) colocalizing with the GFP-labeled *HSP104* gene. An average of 40 cells per timepoint per condition were scored. Graphs depict means + SD. N=2.

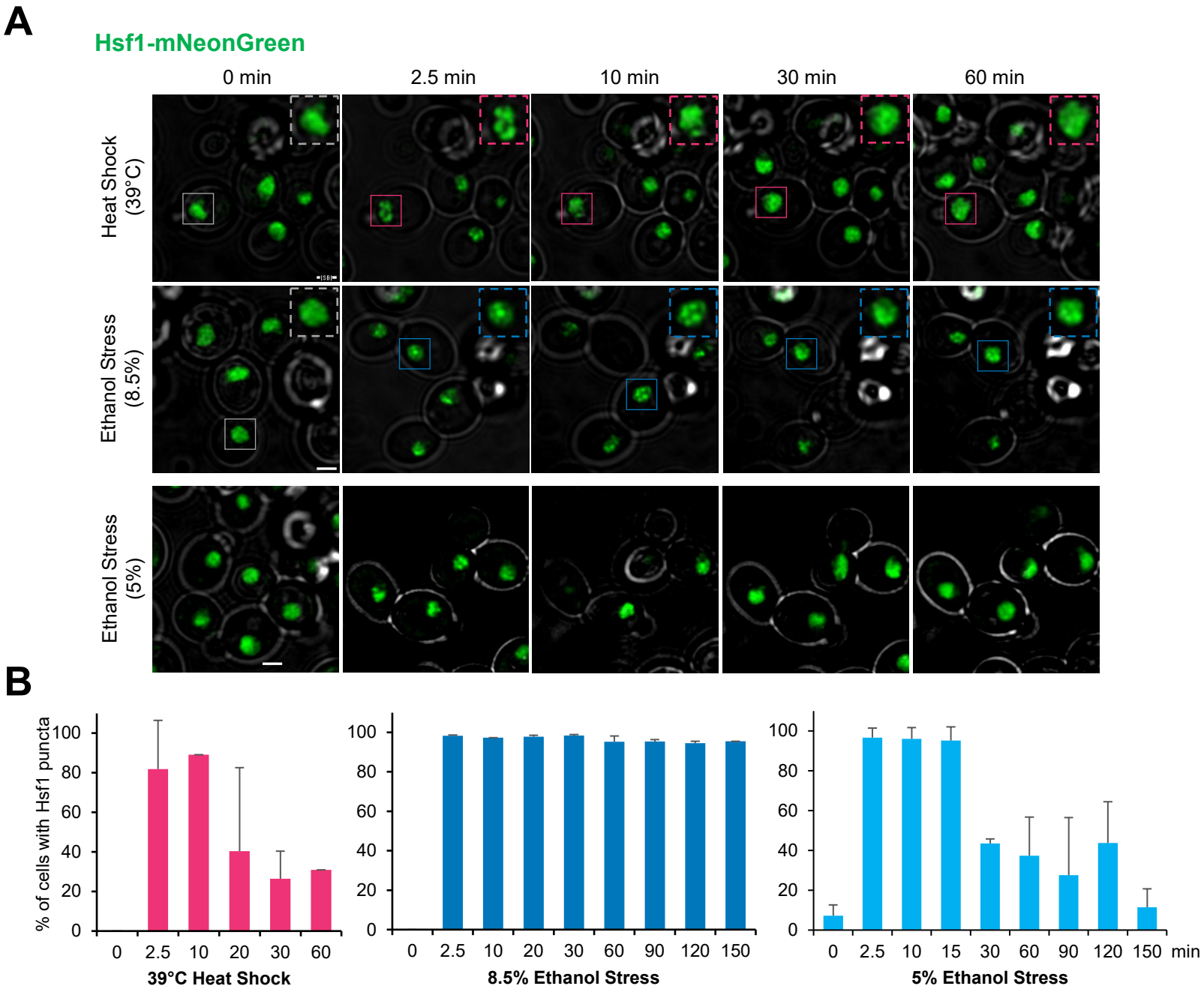

Figure 7–figure supplement 1. Hsf1-mNeonGreen rapidly forms condensates in response to both thermal and ethanol stress.

(A) Visualization of Hsf1-mNeonGreen (LRY040 haploid strain) exposed to heat shock (39°C) or ethanol stress (8.5% or 5% v/v, 25°C). Control (0 min) was kept at 25°C. Single plane is shown, from an 11 z-planes stack taken with 0.5 µm of interplanar distance. Dashed box represents zoom-in of a representative cell for that time point (continuous box). Scale bar: 2 µm

(B) Cells treated as in (A) were scored for the presence of Hsf1-mNeonGreen foci using Imaris software (v.10.0.0. See Materials and Methods). Depicted is the percentage of cells in the population displaying Hsf1 foci. Average cells scored per condition, per timepoint: 150. N=2. Shown are means + SD.

Figure 9–figure supplement 1

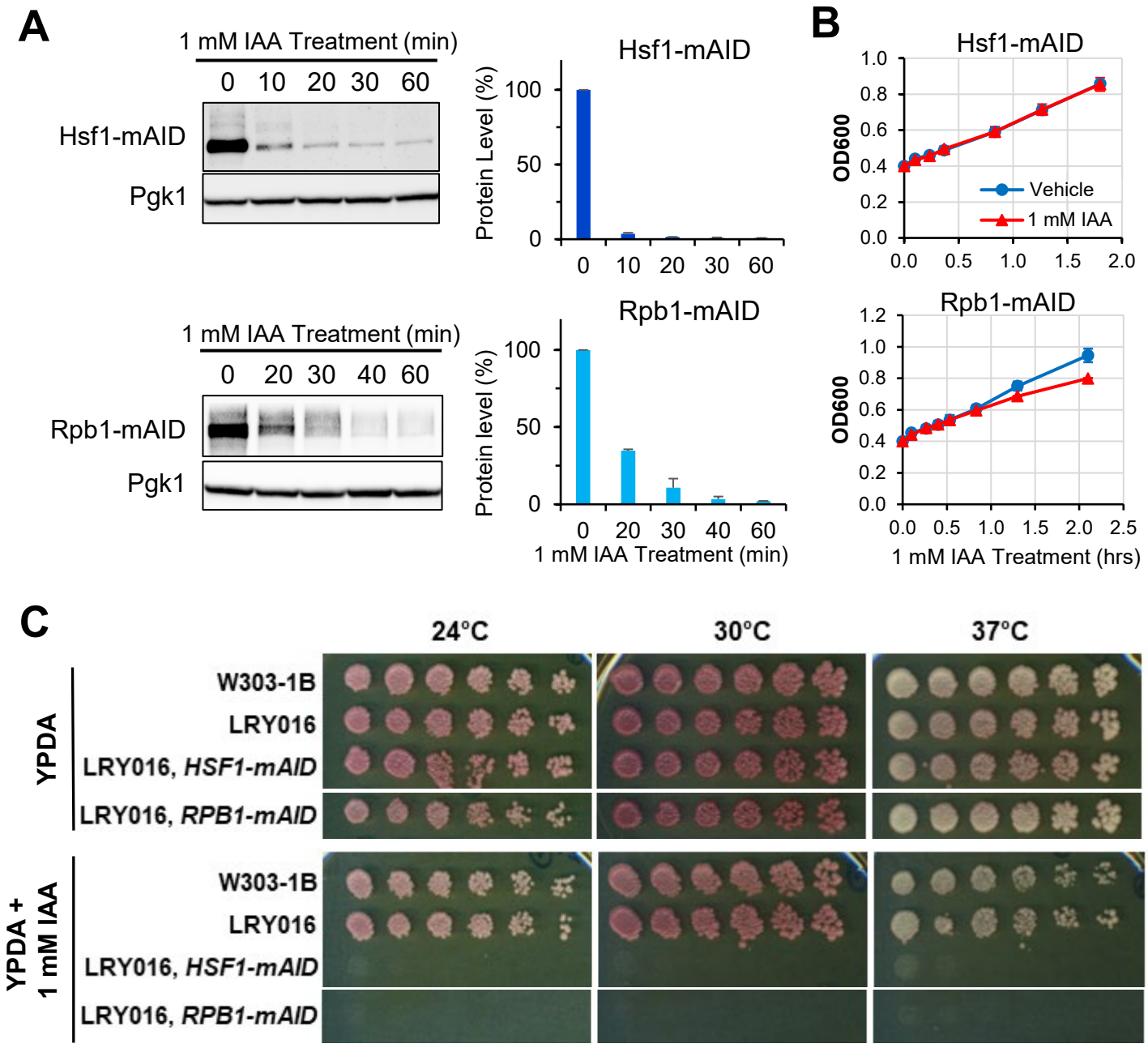

Figure 9–figure supplement 1. Hsf1 and Rpb1 are efficiently degraded in degron-tagged strains following addition of auxin.

(A) Analysis of protein degradation by Immunoblot. Strains LRY100 and LRY102 (Hsf1-mAID and Rpb1-mAID, respectively) were grown in YPDA to mid-log phase and subjected to 1 mM IAA treatment for different lengths of time. Cells were harvested and processed by Western blot. cMyc antibody was used to visualize mAID tagged proteins, endogenous Pgk1 serves as the loading control. Quantification of mAID tagged protein levels is shown on the right. Normalization was done to Pgk1 and 0 min samples. Shown are means + SD. N=2.

(B) Growth curve assay of LRY100 and LRY102 cells exposed to 1 mM IAA. Cells were pre-grown in YPDA to mid-log phase, then diluted with equivalent volume of YPDA + IAA in ethanol (vehicle) for a final concentration of 1 mM IAA and 1.7% ethanol or just 1.7% ethanol (vehicle-treated control). Samples were incubated with shaking at 25°C, aliquots were removed to monitor OD_{600} at the indicated times. Plots depict means + SD. N=2.

(C) Spot dilution analysis of cells from the indicated strains. Cells were pre-grown to early log phase, diluted to OD_{600}=0.5 in autoclaved distilled water, then serially diluted 1:3. A 6x8 applicator was used to spot cells on YPDA or YPDA + 1 mM IAA plates. Incubation was done at the indicated temperatures for 3 days.